

DFTT 32/97
 KIAS-P97004
 hep-ph/9709439

ATMOSPHERIC NEUTRINO OSCILLATIONS WITH THREE NEUTRINOS AND A MASS HIERARCHY

C. Giunti^(a), C.W. Kim^(b) and M. Monteno^(c)

^(a) *INFN, Sezione di Torino, and Dipartimento di Fisica Teorica,
 Università di Torino, Via P. Giuria 1, I-10125 Torino, Italy*

^(b) *Department of Physics and Astronomy, The Johns Hopkins University,
 Baltimore, Maryland 21218, USA, and
 School of Physics, Korea Institute for Advanced Study
 Seoul 130-012, Korea*

^(c) *INFN, Sezione di Torino, and Dipartimento di Fisica Sperimentale,
 Università di Torino, Via P. Giuria 1, I-10125 Torino, Italy*

Abstract

A comprehensive formalism for the description of neutrino oscillations in the Earth in a general scheme with three massive neutrinos and the mass hierarchy $m_1 \ll m_2 \ll m_3$ is presented. Using this formalism, which is valid both in vacuum and in a medium, the matter effect on the oscillations of low-energy neutrinos is discussed, pointing out the existence of very long oscillations which are independent of the neutrino masses and the neutrino energy, and are very sensitive to the matter density along the neutrino trajectory. As an example of application of the formulation, a fit of the Kamiokande atmospheric neutrino data with the matter effect taken into account for neutrinos propagating in the Earth is presented. The results of the fit indicate that $4 \times 10^{-3} \text{ eV}^2 \lesssim m_3^2 \lesssim 4 \times 10^{-2} \text{ eV}^2$ and the oscillation amplitudes in all channels ($\nu_\mu \leftrightarrow \nu_e$, $\nu_\mu \leftrightarrow \nu_\tau$, $\nu_e \leftrightarrow \nu_\tau$) could be large. Hence, long-baseline experiments with reactor (CHOOZ and Palo Verde) and accelerator (K2K, MINOS and ICARUS) neutrinos could observe neutrino oscillations in all channels with a relatively large statistics.

1 Introduction

The atmospheric neutrino anomaly [1, 2, 3, 4, 5] is one of the indications in favor of the existence of neutrino oscillations [6] (see Refs.[7, 8, 9, 10, 11]), a phenomenon which is realized if neutrinos are massive particles and leptons, as in the case of quarks, are mixed (i.e. the mass matrices of the weak-interacting leptons are not diagonal). Neutrino oscillation is considered today one of the most interesting phenomena in high energy physics as well as one of the most promising ways to search new physics beyond the Standard Model (see Ref.[9, 11]).

The atmospheric neutrino anomaly has been observed by the Kamiokande [1, 2, 3], IMB [4] and Soudan [5] experiments, which measured a ratio of contained muon-like to electron-like events smaller than the expected one [12, 13, 14, 15, 16]. The experimental data can be explained by $\nu_\mu \rightarrow \nu_\tau$ or $\nu_\mu \leftrightarrow \nu_e$ oscillations with a neutrino mass-squared difference $\Delta m^2 \sim 10^{-2} \text{ eV}^2$. A preliminary analysis of recent SuperKamiokande data [17] confirms the atmospheric neutrino anomaly, but indicates a smaller value of Δm^2 : $3 \times 10^{-4} \lesssim \Delta m^2 \lesssim 6 \times 10^{-3} \text{ eV}^2$. The anomaly observed by Kamiokande and SuperKamiokande cannot be explained with a background flux of slow neutrons [18, 19, 17]. In this paper, for the sake of definiteness, we use only the Kamiokande data, waiting for definitive data from SuperKamiokande.

On the other hand, no anomaly was observed in the ratio of contained muon-like to electron-like events by the Fréjus [20] and NUSEX [21] experiments and in the ratio of contained muon-like to total events with energy higher than 1 GeV by the IMB experiment [22]. However, the statistical error of the Fréjus and NUSEX data is higher than that of the Kamiokande data and the inclusion in the fit of the data of the Fréjus and NUSEX experiments does not eliminate the necessity of neutrino oscillations [23, 24]. Also the high energy IMB data have relatively large errors and they are not statistically incompatible with the data of the Kamiokande experiment [22]. No anomaly was also observed in the absolute flux of upward-going muons by the Kamiokande [25], IMB [26], Baksan [27] and MACRO¹ [28] experiments. However, the knowledge of the absolute value of the flux of neutrino-induced upward-going muons without neutrino oscillations is rather model-dependent [29] (see Ref.[30] for a combined analysis of the available upward-going muon data).

The neutrino oscillation solution of the atmospheric neutrino anomaly will be checked in the next years by the CHOOZ [31] and Palo Verde [32] long-baseline $\bar{\nu}_e$ disappearance experiments with reactor anti-neutrinos and by the KEK-SuperKamiokande (K2K) [33], Fermilab-Soudan (MINOS) [34] and CERN-Gran Sasso (ICARUS) [35] long-baseline experiments with accelerator neutrinos and anti-neutrinos, which are sensitive to the disappearance of $\bar{\nu}_\mu^{(-)}$ and to $\bar{\nu}_\mu^{(-)} \rightarrow \bar{\nu}_e^{(-)}$ and $\bar{\nu}_\mu^{(-)} \rightarrow \bar{\nu}_\tau^{(-)}$ transitions.

Another important indication in favor of neutrino oscillations comes from the results of

¹ Although the total flux of upward-going muons observed by the MACRO experiment is compatible, within errors, with the calculated one (without neutrino oscillations), the angular shape of the flux does not match the expectations, because of a deficit in the angular bins corresponding to the vertical direction. However, the compatibility of this deficit with neutrino oscillations is still uncertain [28].

the solar neutrino experiments (Homestake [37], Kamiokande [38], GALLEX [39], SAGE [40] and SuperKamiokande [41]), which observed event rates significantly smaller than the values predicted by the Standard Solar Model (SSM) [42, 43, 44, 45]. Moreover, the experimental data indicate that the suppression of solar ν_e 's depends on energy, excluding an astrophysical solution of the solar neutrino problem [46]. Assuming the validity of the SSM, the experimental data can be described by MSW resonant transitions [47] with $\Delta m^2 \sim 10^{-5} \text{ eV}^2$ [48] or by vacuum oscillations with $\Delta m^2 \sim 10^{-10} \text{ eV}^2$ [49] (Δm^2 is a neutrino mass-squared difference).

A solution of the solar and atmospheric neutrino problem with neutrino oscillations requires the existence of two different scales of neutrino mass-squared differences, which corresponds to the existence of three massive neutrinos, ν_1 , ν_2 and ν_3 , with masses m_1 , m_2 and m_3 , respectively. These three massive neutrinos are mixings of the three flavor neutrinos, ν_e , ν_μ and ν_τ , whose existence is known² from the measurements of the invisible width of the Z boson done by LEP experiments (see Ref.[50]).

The experimental upper bounds on the values of the neutrino masses (see Refs.[51, 50]) imply that the neutrino masses are much smaller than the masses of the corresponding charged leptons. An attractive theoretical explanation of this smallness is given by the see-saw mechanism [36], which allows the hierarchical pattern (see Refs.[8, 9, 10, 11])

$$m_1 \ll m_2 \ll m_3. \quad (1.1)$$

This is the simplest and most natural scheme for the neutrino masses, analogous to the mass-schemes of charged leptons, up and down quarks, all of which have a hierarchy of masses. The hierarchical scheme (1.1) is exactly what is needed for a neutrino oscillation solution of the solar and atmospheric neutrino problems, if $m_2^2 \sim 10^{-5}$ or 10^{-10} eV^2 (for the MSW or vacuum oscillation solution of the solar neutrino problem) and $m_3^2 \sim 10^{-2} \text{ eV}^2$ (for the solution of the atmospheric neutrino anomaly). In this paper we consider this possibility [23, 24] and we present a comprehensive formalism for the description of atmospheric neutrino oscillations, by taking into account the matter effect [52, 47] for neutrinos propagating in the Earth [53, 54]. We believe that this formalism will be useful for the analysis of the atmospheric neutrino data of the next generation of experiments, especially those of the SuperKamiokande experiment.

Recently the LSND collaboration reported [55] the observation of anomalous $\bar{\nu}_e p \rightarrow e^+ n$ events produced by neutrinos originating from μ^+ decays at rest. These events could be explained by $\bar{\nu}_\mu \rightarrow \bar{\nu}_e$ oscillations with $\Delta m^2 \sim 1 \text{ eV}^2$, but this possibility is excluded in the schemes with three neutrinos if the neutrino masses have the values appropriate for the explanation of the solar and atmospheric neutrino problem [56]. In this paper we do not consider the LSND indication in favor of neutrino oscillations, waiting for its confirmation by other experiments (KARMEN [57] and others [58]).

In Section 3 we present our fit of the Kamiokande data in the scheme (1.1), with the assumption that $m_2^2 \sim 10^{-5}$ or 10^{-10} eV^2 , so that $\Delta m_{21}^2 \equiv m_2^2 - m_1^2 \simeq m_2^2$ is relevant for the

² The tau neutrino has not been directly observed, but it is widely believed to exist without doubt because it is necessary for the consistency of the Standard Model of electro-weak interactions.

oscillations of solar neutrinos. With these assumptions, the oscillations of atmospheric neutrinos depend only on $\Delta m_{31}^2 \equiv m_3^2 - m_1^2 \simeq m_3^2$.

In the analysis of the experimental indications in favor of neutrino oscillations one must take into account also the numerous negative results of the terrestrial neutrino oscillation experiments with reactor $\bar{\nu}_e$'s and accelerator ν_μ 's and $\bar{\nu}_\mu$'s (the latest results are summarized in Ref.[59]). In particular, in Section 3.3 it will be shown that part of the region of neutrino mixing parameters allowed by the atmospheric neutrino data is excluded by the results of the Bugey [60] and Krasnoyarsk [61] reactor $\bar{\nu}_e$ disappearance experiment.

The plan of the paper is as follows. In Section 2 we present the general formalism for the description of oscillations of three neutrinos in vacuum and in matter. In Section 2.1 we mainly discuss the oscillations of atmospheric neutrinos in the scheme (1.1) with three neutrinos and a mass hierarchy. In Section 2.2 we discuss the matter effect on the oscillations of neutrinos with low energy. In Section 3 we present our fit of the Kamiokande atmospheric data. In Section 4 we draw our conclusions. In the Appendix A we present a derivation of the parameterization of the mixing matrix used in the paper.

2 Oscillations of 3 neutrinos

The theory of neutrino mixing (see Refs.[7, 8, 9, 10, 11]) is based on the hypothesis that the left-handed flavor neutrino fields $\nu_{\alpha L}$ are superpositions of the left-handed components of (Dirac or Majorana) massive neutrino fields ν_{kL} :

$$\nu_{\alpha L} = \sum_k U_{\alpha k} \nu_{kL} , \quad (2.1)$$

where U is a unitary mixing matrix ($UU^\dagger = U^\dagger U = 1$).

The results of the LEP experiments on the measurement of the invisible width of the Z boson (see Ref.[50]) imply that only three "light" active flavor neutrinos exist in nature, i.e. ν_e , ν_μ and ν_τ . However, the existence of sterile flavor neutrinos is not ruled out and the number of neutrinos with a definite mass is unknown. We will consider here the simplest scenario with only three active flavor neutrinos and three (Dirac or Majorana) neutrinos with definite mass. Hence, in the following we will consider the flavor indices $\alpha, \beta, \rho, \sigma = e, \mu, \tau$ and the mass indices $k, j = 1, 2, 3$.

A neutrino with momentum p produced by a charged-current weak interaction process together with a charged lepton α is described by a flavor state $|\nu_\alpha(p)\rangle$, which is a superposition of neutrino mass eigenstates $|\nu_k(p)\rangle$:

$$|\nu_\alpha(p)\rangle = \sum_k U_{\alpha k}^* |\nu_k(p)\rangle . \quad (2.2)$$

The state $|\nu_k(p)\rangle$ describes a neutrino with a definite mass m_k , momentum p , energy $E_k = \sqrt{p^2 + m_k^2}$, and satisfies the energy eigenvalue equation

$$\mathcal{H}_0 |\nu_k(p)\rangle = E_k |\nu_k(p)\rangle , \quad (2.3)$$

where \mathcal{H}_0 is the free neutrino Hamiltonian. Since the neutrino masses are very small, the detectable neutrinos are extremely relativistic and the approximation $E_k \simeq p + m_k^2/2p$ is allowed.

In this paper we consider atmospheric neutrinos, which are produced at the top of the atmosphere by the interaction of primary cosmic rays with the nuclei in the air (see Ref.[13]). Atmospheric neutrinos propagate in the atmosphere, which is practically equivalent to vacuum, and in the interior of the Earth, where the matter density is sufficiently high to modify the effective energy-momentum dispersion relation through the coherent interaction with the particles in the medium [52, 53, 54]. In the following part of this Section we derive the evolution equation for the transition amplitudes between flavor states which is valid both in vacuum and in matter.

For neutrinos propagating in matter, the Hamiltonian \mathcal{H} is given by

$$\mathcal{H} = \mathcal{H}_0 + \mathcal{H}_I, \quad (2.4)$$

where \mathcal{H}_I is the effective weak interaction Hamiltonian due to the coherent interaction with the electrons, protons and neutrons in a medium. The flavor states (2.2) are eigenstates of \mathcal{H}_I :

$$\mathcal{H}_I |\nu_\alpha(p)\rangle = V_\alpha |\nu_\alpha(p)\rangle, \quad (2.5)$$

with

$$V_e = V_{CC} + V_{NC}, \quad V_\mu = V_\tau = V_{NC}. \quad (2.6)$$

Here V_{CC} and V_{NC} are, respectively, the charged-current and neutral-current effective potentials of neutrinos, given by

$$V_{CC} = \sqrt{2} G_F N_e, \quad V_{NC} = -\frac{\sqrt{2}}{2} G_F N_n, \quad (2.7)$$

where G_F is the Fermi constant and N_e and N_n are, respectively, the electron and neutron number densities of the medium³. The effective potentials of anti-neutrinos have the same absolute value, but opposite sign: $\bar{V}_{CC} = -V_{CC}$, $\bar{V}_{NC} = -V_{NC}$.

Let us consider a neutrino with momentum p produced at the time $t = 0$ by a charged-current weak interaction process together with a charged lepton α ($\alpha = e, \mu, \tau$). In the Schrödinger picture, at the time t this neutrino is described by the state

$$|\varphi^{(\alpha)}(p, t)\rangle = \sum_{\beta} \varphi_{\beta}^{(\alpha)}(p, t) |\nu_{\beta}(p)\rangle. \quad (2.8)$$

This state is a superposition of flavor states $|\nu_{\beta}(p)\rangle$ with amplitudes $\varphi_{\beta}^{(\alpha)}(p, t)$ which depend on time and have the initial value $\varphi_{\beta}^{(\alpha)}(p, 0) = \delta_{\alpha\beta}$.

³ Here we consider an electrically neutral medium, in which the number density of protons is equal to the number density of electrons. This implies that the neutral-current effective potentials of protons and electrons cancel each other.

The time evolution of the state (2.8) is given by the Schrödinger equation

$$\begin{aligned}
i \frac{d}{dt} |\varphi^{(\alpha)}(p, t)\rangle &= \mathcal{H} |\varphi^{(\alpha)}(p, t)\rangle = \sum_{\rho} \varphi_{\rho}^{(\alpha)}(p, t) (\mathcal{H}_0 + \mathcal{H}_I) |\nu_{\rho}(p)\rangle \\
&= \sum_{\rho} \varphi_{\rho}^{(\alpha)}(p, t) \left(\sum_k U_{\rho k}^* E_k |\nu_k(p)\rangle + V_{\rho} |\nu_{\rho}(p)\rangle \right) \\
&= \sum_{\sigma, \rho} \varphi_{\rho}^{(\alpha)}(p, t) \left(\sum_k U_{\rho k}^* E_k U_{\sigma k} + V_{\rho} \delta_{\rho\sigma} \right) |\nu_{\sigma}(p)\rangle .
\end{aligned} \tag{2.9}$$

Projecting this equation on $\langle \nu_{\beta}(p) |$ and taking into account that $\langle \nu_{\beta}(p) | \nu_{\rho}(p) \rangle = \delta_{\beta\rho}$, we obtain

$$i \frac{d}{dt} \varphi_{\beta}^{(\alpha)}(p, t) = \sum_{\rho} \left(\sum_k U_{\beta k} E_k U_{\rho k}^* + V_{\rho} \delta_{\beta\rho} \right) \varphi_{\rho}^{(\alpha)}(p, t) . \tag{2.10}$$

This is the evolution equation for the flavor amplitudes $\varphi_{\beta}^{(\alpha)}(p, t)$, whose squared-modulus gives the probability of $\nu_{\alpha} \rightarrow \nu_{\beta}$ transitions: $P_{\nu_{\alpha} \rightarrow \nu_{\beta}}(p, t) = \left| \varphi_{\beta}^{(\alpha)}(p, t) \right|^2$.

For relativistic neutrinos we have

$$i \frac{d}{dt} \varphi_{\beta}^{(\alpha)}(p, t) = (p + V_{NC}) \varphi_{\beta}^{(\alpha)}(p, t) + \sum_{\rho} \left(\sum_k U_{\beta k} \frac{m_k^2}{2p} U_{\rho k}^* + V_{CC} \delta_{\beta e} \delta_{\rho e} \right) \varphi_{\rho}^{(\alpha)}(p, t) , \tag{2.11}$$

where we have separated the contribution of the neutral-current effective potential V_{NC} , which is the same for the three neutrino flavors, from the contribution of the charged-current effective potential V_{CC} , which affects only the electron neutrino component. The time t is equal (in natural units) to the distance L of propagation of the neutrino.

Since neutrino oscillations are due to the difference of the phases of different mass eigenstates, in the following we consider the simplified evolution equation for the amplitudes

$$\psi_{\beta}^{(\alpha)}(p, t) \equiv \varphi_{\beta}^{(\alpha)}(p, t) \exp \left(i p t + i \int_0^t V_{NC}(t') dt' \right) , \tag{2.12}$$

where we have taken into account the fact that V_{NC} may not be constant along the neutrino trajectory. For relativistic neutrinos we have

$$i \frac{d}{dt} \psi_{\beta}^{(\alpha)}(p, t) = \sum_{\rho} \left(\sum_k U_{\beta k} \frac{m_k^2}{2p} U_{\rho k}^* + V_{CC} \delta_{\beta e} \delta_{\rho e} \right) \psi_{\rho}^{(\alpha)}(p, t) . \tag{2.13}$$

This is the evolution equation for the transition amplitudes $\psi_{\beta}^{(\alpha)}(p, t)$, which allows one to calculate the oscillation probabilities in vacuum ($V_{CC} = 0$) as well as in matter ($V_{CC} \neq 0$).

The probability to detect a neutrino with flavor β after a time t , which corresponds to a propagation distance $L = t$, is given by

$$P_{\nu_\alpha \rightarrow \nu_\beta}(p, t) = \left| \varphi_\beta^{(\alpha)}(p, t) \right|^2 = \left| \psi_\beta^{(\alpha)}(p, t) \right|^2. \quad (2.14)$$

The solution of the evolution equation (2.13) in vacuum is simply given by

$$\psi_\beta^{(\alpha)}(p, t) = \sum_k U_{\alpha k}^* U_{\beta k} \exp \left(-i \frac{m_k^2}{2p} t \right). \quad (2.15)$$

The application of Eq.(2.14) leads to the well known formula for the oscillation probabilities

$$P_{\nu_\alpha \rightarrow \nu_\beta}(p, t) = \sum_k |U_{\alpha k}|^2 |U_{\beta k}|^2 + 2 \operatorname{Re} \sum_{k>j} U_{\alpha k}^* U_{\beta k} U_{\alpha j} U_{\beta j}^* \exp \left(-i \frac{\Delta m_{kj}^2}{2p} t \right), \quad (2.16)$$

with $\Delta m_{kj}^2 \equiv m_k^2 - m_j^2$.

We now derive a method for the solution of the evolution equation (2.13) in matter. It is convenient to write the evolution equation (2.13) in matrix form:

$$i \frac{d}{dt} \Psi_W^{(\alpha)}(p, t) = \frac{1}{2p} (U M^2 U^\dagger + A_W) \Psi_W^{(\alpha)}(p, t), \quad (2.17)$$

where

$$\Psi_W^{(\alpha)}(p, t) \equiv \begin{pmatrix} \psi_e^{(\alpha)}(p, t) \\ \psi_\mu^{(\alpha)}(p, t) \\ \psi_\tau^{(\alpha)}(p, t) \end{pmatrix}, \quad M \equiv \operatorname{diag}(m_1, m_2, m_3), \quad A_W \equiv \operatorname{diag}(A_{CC}, 0, 0), \quad (2.18)$$

and $A_{CC} \equiv 2pV_{CC}$. For anti-neutrinos, A_{CC} must be replaced by $\bar{A}_{CC} = -A_{CC}$.

The 3×3 mixing matrix U can be written in the form (see the Appendix A)

$$U = V_{23} V_{13} W_{12} D(\lambda), \quad (2.19)$$

with the orthogonal matrices

$$V_{23} = \begin{pmatrix} 1 & 0 & 0 \\ 0 & \cos \vartheta_{23} & \sin \vartheta_{23} \\ 0 & -\sin \vartheta_{23} & \cos \vartheta_{23} \end{pmatrix}, \quad V_{13} = \begin{pmatrix} \cos \vartheta_{13} & 0 & \sin \vartheta_{13} \\ 0 & 1 & 0 \\ -\sin \vartheta_{13} & 0 & \cos \vartheta_{13} \end{pmatrix}, \quad (2.20)$$

and the unitary matrices

$$W_{12} = D_{12} V_{12} D_{12}^\dagger, \quad D(\lambda) = \operatorname{diag}(e^{i\lambda_1}, e^{i\lambda_2}, 1), \quad (2.21)$$

with

$$V_{12} = \begin{pmatrix} \cos \vartheta_{12} & \sin \vartheta_{12} & 0 \\ -\sin \vartheta_{12} & \cos \vartheta_{12} & 0 \\ 0 & 0 & 1 \end{pmatrix}, \quad D_{12} = \text{diag}(e^{i\eta_{12}}, 1, 1). \quad (2.22)$$

Here ϑ_{23} , ϑ_{13} , and ϑ_{12} are the three mixing angles, η_{12} is the Dirac CP-violating phase [62] and λ_1 and λ_2 are the two Majorana CP-violating phases. The matrix V_{ab} represents a rotation of an angle ϑ_{ab} in the ν_a - ν_b plane. In the case of Dirac neutrinos the matrix $D(\lambda)$ containing the two Majorana CP-violating phases can be eliminated with a suitable redefinition of the arbitrary phases of the Dirac neutrino fields. This operation is not possible for Majorana neutrinos because the Majorana mass term is not invariant under rephasing of the neutrino fields. However, the presence of the matrix $D(\lambda)$ does not have any effect on neutrino oscillations in vacuum [64, 66] as well as in matter [67]. Indeed, from Eq.(2.17) it is clear that neutrino oscillations depend on the quantity $U M^2 U^\dagger$ and, since the diagonal matrix M^2 commutes with the diagonal matrix $D(\lambda)$, we have

$$U M^2 U^\dagger = V_{23} V_{13} W_{12} D(\lambda) M^2 D(\lambda)^\dagger W_{12}^\dagger V_{13}^\dagger V_{23}^\dagger = V_{23} V_{13} W_{12} M^2 W_{12}^\dagger V_{13}^\dagger V_{23}^\dagger. \quad (2.23)$$

Contrary to the Majorana phases, the Dirac phase η_{12} , contained in W_{12} , has an effect on neutrino oscillations [68]. Under CP transformations $U \xrightarrow{\text{CP}} U^*$, which is equivalent to $\eta_{12} \xrightarrow{\text{CP}} -\eta_{12}$. This means that CP violation could be observed in neutrino oscillations, measuring the differences $P_{\nu_\alpha \rightarrow \nu_\beta} - P_{\bar{\nu}_\alpha \rightarrow \bar{\nu}_\beta}$ for $\alpha \neq \beta$ (CPT invariance implies that $P_{\nu_\alpha \rightarrow \nu_\beta} = P_{\bar{\nu}_\beta \rightarrow \bar{\nu}_\alpha}$ and therefore $P_{\nu_\alpha \rightarrow \nu_\alpha} - P_{\bar{\nu}_\alpha \rightarrow \bar{\nu}_\alpha}$ is always equal to zero). Assuming CPT invariance, a violation of CP implies a violation of T, which could be observed by measuring the difference $P_{\nu_\alpha \rightarrow \nu_\beta} = P_{\nu_\beta \rightarrow \nu_\alpha}$ for $\alpha \neq \beta$.

The fact that the matrix A_W has only one non-zero element $(A_W)_{11} = A_{CC}$ implies that

$$V_{23}^\dagger A_W V_{23} = A_W. \quad (2.24)$$

Therefore, it is convenient to define the new column matrix of amplitudes

$$\widetilde{\Psi}^{(\alpha)}(p, t) \equiv V_{23}^\dagger \Psi_W^{(\alpha)}(p, t), \quad (2.25)$$

which satisfy the simplified evolution equation

$$i \frac{d}{dt} \widetilde{\Psi}^{(\alpha)}(p, t) = \frac{\widetilde{M}^2}{2p} \widetilde{\Psi}^{(\alpha)}(p, t), \quad (2.26)$$

with

$$\widetilde{M}^2 = V_{13} W_{12} M^2 W_{12}^\dagger V_{13}^\dagger + A_W. \quad (2.27)$$

Notice that the amplitudes in the column matrix $\widetilde{\Psi}^{(\alpha)}(p, t)$ do not have a definite flavor or mass character. They are introduced only as a tool for the solution of the evolution equation (2.17).

The standard procedure that has been used in finding the solution of Eq.(2.26) consists of the diagonalization of the effective squared-mass matrix \widetilde{M}^2 (see Refs.[54, 10]). This method is appropriate for a constant matter density or for a medium whose density changes along the path of neutrino propagation are much slower than the changes of the oscillation phases (adiabatic approximation). Techniques have been developed in order to extend the solution to non-adiabatic cases in which the matter density have a smooth and monotonic variation (as is the case for solar neutrinos; see Refs.[54, 10]). However, the general case of irregular matter variations must be solved by integrating numerically Eq.(2.26) (or directly Eq.(2.17)).

In the following we consider neutrino oscillations in the Earth, whose internal composition is well approximated by a number of shells with constant density (see Refs.[69, 70]). The solid curve in Fig.1A shows the density ρ in the interior of the Earth as a function of the radial distance r from the center of the Earth according to the data given in Ref.[70]. The dotted curve represents our approximation in terms of five shells with constant densities $\rho_{i=1,\dots,5} = 13.0, 11.3, 5.0, 3.9, 3.0 \text{ g/cm}^3$, with outer radii $r_{i=1,\dots,5} = 1221, 3480, 5701, 5971, 6371 \text{ Km}$. The solid curve in Fig.1B shows the electron number density $N_e = \rho \langle Z/A \rangle$ as a function of the radial distance r and the dotted curve represents our approximation in terms of five shells with constant electron number density $(N_e)_{i=1,\dots,5} = 6.15, 5.36, 2.47, 1.93, 1.50 \text{ N}_A \text{ cm}^{-3}$. For the averaged ratio $\langle Z/A \rangle$ we took $\langle Z/A \rangle_{1,2} = 0.475$ for the two inner shells (core) and $\langle Z/A \rangle_{3,4,5} = 0.495$ for the three outer shells (mantle).

The effective squared-mass matrix \widetilde{M}^2 can be diagonalized separately in each shell, yielding a relatively simple solution for the evolution equation (2.26) in the shell under consideration. The solutions in confining shells are matched on the shell boundaries by the continuity of the flavor states, which imply the continuity of the amplitudes $\Psi_W^{(\alpha)}(p, t)$ and, from Eq.(2.25), of the amplitudes $\widetilde{\Psi}^{(\alpha)}(p, t)$ (the transformation (2.25) does not depend on the matter density).

In the following we consider a scheme with the hierarchy (1.1) for the neutrino masses. In this case the oscillations of atmospheric neutrinos depend only on one mass scale. This scheme allows a relatively simple diagonalization of the 3×3 effective squared-mass matrix \widetilde{M}^2 .

2.1 One mass scale

We will consider here a scheme with three neutrinos and the hierarchy (1.1) for the neutrino masses. We will assume that the squared-mass difference $\Delta m_{21}^2 \equiv m_2^2 - m_1^2 \simeq m_2^2$ is relevant for the explanation of the solar neutrino problem ($\Delta m_{21}^2 \sim 10^{-5} \text{ eV}^2$ [48] for MSW resonant transitions or $\Delta m_{21}^2 \sim 10^{-10} \text{ eV}^2$ [49] for vacuum oscillations). In this

case

$$\frac{m_1^2 R_\oplus}{2p} \ll 1, \quad \frac{m_2^2 R_\oplus}{2p} \ll 1, \quad (2.28)$$

where $R_\oplus = 6371$ Km is the radius of the Earth, which represents a characteristic distance of propagation for atmospheric neutrinos. Hence, the phases generated by m_1^2 and m_2^2 can be neglected for atmospheric neutrinos and the squared-mass matrix M^2 can be approximated with

$$M^2 = \text{diag}(0, 0, m_3^2). \quad (2.29)$$

Before proceeding with the derivation of the oscillation probabilities that follow from this approximation, it is necessary to notice that caution is needed for low-energy atmospheric neutrinos if $m_2^2 \gtrsim 10^{-5} \text{ eV}^2$, because in this case $m_2^2 R_\oplus / 2p \ll 1$ only for $p \gg 150$ MeV. According to the most recent analyses of the solar neutrino data [71], including preliminary data from SuperKamiokande [41], the small and large mixing angle MSW solutions of the solar neutrino problem require, respectively, $4 \times 10^{-6} \text{ eV}^2 \lesssim m_2^2 \lesssim 1.2 \times 10^{-5} \text{ eV}^2$ and $9 \times 10^{-6} \text{ eV}^2 \lesssim m_2^2 \lesssim 3 \times 10^{-5} \text{ eV}^2$ at 90% CL. Hence, especially in the case of the large mixing angle MSW solution of the solar neutrino problem, the formalism described in this section may be not applicable to low-energy atmospheric neutrinos (as, for example, some part of those contributing to the Kamiokande and SuperKamiokande sub-GeV data). Since, as will be discussed later, the formalism described in this section is very convenient for the analysis of atmospheric neutrino data in the case of three-neutrino mixing (the oscillation probabilities are independent from ϑ_{12} and η_{12}), we think that if a high value of m_2^2 will be established, it will be convenient to analyze the atmospheric neutrino data with a cut in energy such that $m_2^2 R_\oplus / 2p \ll 1$ (at least for a first analysis, before the calculation of a complete fit which should include also the solar neutrino data for the determination of m_2^2 and ϑ_{12}). Let us emphasize that there are good hopes that the value of $m_2^2 \simeq \Delta m_{21}^2$ will be determined by the new generation of solar neutrino experiments (SuperKamiokande, SNO, ICARUS, Borexino, GNO and others [72]) that are expected to be able to distinguish among the different solutions of the solar neutrino problem.

The simple form of the squared-mass matrix (2.29) allows one to write the oscillation probabilities in vacuum in an elegant way: using the unitarity relation

$$\sum_{k=1,2} U_{\beta k} U_{\alpha k}^* = \delta_{\alpha\beta} - U_{\beta 3} U_{\alpha 3}^*, \quad (2.30)$$

the amplitudes (2.15) can be written as

$$\begin{aligned} \psi_\beta^{(\alpha)}(p, t) &= \left(\sum_{k=1,2} U_{\alpha k}^* U_{\beta k} \right) + U_{\alpha 3}^* U_{\beta 3} \exp \left(-i \frac{m_3^2 t}{2p} \right) \\ &= \delta_{\alpha\beta} + U_{\alpha 3}^* U_{\beta 3} \left[\exp \left(-i \frac{m_3^2 t}{2p} \right) - 1 \right]. \end{aligned} \quad (2.31)$$

For the oscillation probabilities we obtain [73, 74]

$$P_{\nu_\alpha \rightarrow \nu_\beta} = A_{\alpha;\beta} \sin^2 \left(\frac{m_3^2 t}{4p} \right) \quad (\beta \neq \alpha), \quad (2.32a)$$

$$P_{\nu_\alpha \rightarrow \nu_\alpha} = 1 - \sum_{\beta \neq \alpha} P_{\nu_\alpha \rightarrow \nu_\beta} = 1 - B_{\alpha;\alpha} \sin^2 \left(\frac{m_3^2 t}{4p} \right), \quad (2.32b)$$

where

$$A_{\alpha;\beta} = 4 |U_{\alpha 3}|^2 |U_{\beta 3}|^2, \quad (2.33a)$$

$$B_{\alpha;\alpha} = \sum_{\beta \neq \alpha} A_{\alpha;\beta} = 4 |U_{\alpha 3}|^2 (1 - |U_{\alpha 3}|^2) \quad (2.33b)$$

are the classical oscillation amplitudes.

It is important to notice the following features of the oscillation probabilities (2.32):

1. All oscillation channels ($\nu_\mu \leftrightarrow \nu_e$, $\nu_\mu \leftrightarrow \nu_\tau$, $\nu_e \leftrightarrow \nu_\tau$) are open and have the same oscillation length

$$L_{\text{osc}} = \frac{4\pi p}{m_3^2}. \quad (2.34)$$

2. The transition probabilities are determined by three parameters: m_3^2 , $|U_{e3}|^2$ and $|U_{\mu 3}|^2$ (from the unitarity of the mixing matrix it follows that $|U_{\tau 3}|^2 = 1 - |U_{e3}|^2 - |U_{\mu 3}|^2$). The expression of $|U_{e3}|^2$ and $|U_{\mu 3}|^2$ in terms of the mixing angles of the parameterization (2.19) is

$$|U_{e3}|^2 = \sin^2 \vartheta_{13}, \quad |U_{\mu 3}|^2 = \cos^2 \vartheta_{13} \sin^2 \vartheta_{23}. \quad (2.35)$$

Hence, the oscillation probabilities depend on the two mixing angles ϑ_{13} and ϑ_{23} and do not depend on the value of the mixing angle ϑ_{12} and of the Dirac CP violating phase η_{12} . Since this fact is due to the degeneracy of the first two squared mass eigenvalues in Eq.(2.29), it remains valid for the oscillations in matter (see Eq.(2.49)).

3. The expressions (2.32) have the same form as the standard expressions for the oscillation probabilities in the case of mixing between two massive neutrino fields (see Refs.[7, 8, 9, 10, 11]):

$$P_{\nu_\alpha \rightarrow \nu_\beta} = \sin^2 2\vartheta \sin^2 \left(\frac{\Delta m^2 t}{4p} \right) \quad (\beta \neq \alpha), \quad (2.36a)$$

$$P_{\nu_\alpha \rightarrow \nu_\alpha} = 1 - \sin^2 2\vartheta \sin^2 \left(\frac{\Delta m^2 t}{4p} \right), \quad (2.36b)$$

where Δm^2 is the neutrino mass-squared difference and ϑ is the two-generation mixing angle. In the case of two-neutrino mixing only oscillations between two flavors are

possible and the oscillation probabilities are characterized by two parameters, Δm^2 (which determines the oscillation length $L_{\text{osc}} = 4\pi p/\Delta m^2$) and $\sin^2 2\vartheta$. The important difference between the two-neutrino mixing scheme and the scheme with three-neutrino mixing and a mass hierarchy that we consider here is that the second scheme allows simultaneous transitions among all three flavor neutrinos ($\nu_\mu \leftrightarrow \nu_e$, $\nu_\mu \leftrightarrow \nu_\tau$, $\nu_e \leftrightarrow \nu_\tau$).

4. The equality in the form of the oscillation probabilities in the two-neutrino mixing scheme and in the three-neutrino mixing scheme (1.1) is very important, because the data of all terrestrial oscillation experiments with reactor and accelerator neutrinos have been analyzed by the experimental collaborations under the assumption of two-generation mixing, obtaining constraints on the possible values of the mixing parameters Δm^2 and $\sin^2 2\vartheta$. The results of the analysis of the experimental data are presented in the form of allowed (or excluded) regions in the $\sin^2 2\vartheta$ - Δm^2 plane. Identifying the appropriate $A_{\alpha;\beta}$ or $B_{\alpha;\alpha}$ with $\sin^2 2\vartheta$ and m_3^2 with Δm^2 , the results of the standard analyses of the neutrino oscillation data yield allowed (or excluded) regions in the $A_{\alpha;\beta}$ - m_3^2 and $B_{\alpha;\alpha}$ - m_3^2 planes (with $\alpha, \beta = e, \mu, \tau$).
5. Since the classical oscillation amplitudes (2.33) depend only on the squared moduli of the elements of the mixing matrix and $A_{\beta;\alpha} = A_{\alpha;\beta}$, it is clear that

$$P_{\nu_\alpha \rightarrow \nu_\beta} = P_{\bar{\nu}_\alpha \rightarrow \bar{\nu}_\beta}, \quad (2.37a)$$

$$P_{\nu_\alpha \rightarrow \nu_\beta} = P_{\nu_\beta \rightarrow \nu_\alpha}. \quad (2.37b)$$

Hence, if neutrino oscillations depend only on one mass scale, CP and T violations are not observable. This is true for neutrino oscillations in vacuum as well as in matter, although in matter Eq.(2.37a) is no longer satisfied (see Eq.(2.38) and the following discussion).

Let us now consider oscillations in matter and discuss how to solve the evolution equation (2.26). The form (2.29) for the mass matrix implies that $W_{12} M^2 W_{12}^\dagger = M^2$ and the evolution equation (2.17) does not depend on the value of the mixing angle ϑ_{12} and of the Dirac CP violating phase η_{12} . Then, from Eq.(2.27) we have

$$\widetilde{M}^2 = V_{13} M^2 V_{13}^\dagger + A_W = \begin{pmatrix} m_3^2 \sin^2 \vartheta_{13} + A_{CC} & 0 & m_3^2 \cos \vartheta_{13} \sin \vartheta_{13} \\ 0 & 0 & 0 \\ m_3^2 \cos \vartheta_{13} \sin \vartheta_{13} & 0 & m_3^2 \cos^2 \vartheta_{13} \end{pmatrix} \quad (2.38)$$

The disappearance of the Dirac CP violating phase η_{12} from the evolution equation for the transition amplitudes implies that, in the scheme under consideration, CP violation is not observable in neutrino oscillations in matter, as well as in vacuum. Let us emphasize, however, that, contrary to the vacuum case, in matter the survival and transition probabilities of neutrinos and anti-neutrinos can be different, because the effective potentials of neutrinos and anti-neutrinos have the same absolute value but opposite signs. Hence, Eq.(2.37a) is not satisfied in matter. This is due to the fact that the medium is not CP

invariant and not CPT invariant. However, if the matter distribution is symmetric along the neutrino path, the matter effect is T invariant and $P_{\nu_\alpha \rightarrow \nu_\beta} = P_{\nu_\beta \rightarrow \nu_\alpha}$ in matter as in vacuum (see Eq.(2.37b)).

Let us now proceed to diagonalize the matrix \widetilde{M}^2 in Eq.(2.38). Obviously, the matrix \widetilde{M}^2 has a zero eigenvalue, $m_{M2}^2 = 0$. The other two eigenvalues are given by

$$m_{M1,3}^2 = \frac{1}{2} (m_3^2 + A_{CC}) \mp \frac{1}{2} \sqrt{(m_3^2 \cos 2\vartheta_{13} - A_{CC})^2 + (m_3^2 \sin 2\vartheta_{13})^2}. \quad (2.39)$$

These are the effective squared-masses of neutrinos propagating in matter. Notice that the values of the effective squared-masses of neutrinos and anti-neutrinos, which we will denote as $\bar{m}_{M1,3}^2$, are different, because $\bar{A}_{CC} = -A_{CC}$.

Let us define the column matrix of amplitudes

$$\begin{pmatrix} \psi_{M1}^{(\alpha)}(p, t) \\ \psi_{M2}^{(\alpha)}(p, t) \\ \psi_{M3}^{(\alpha)}(p, t) \end{pmatrix} \equiv \Psi_M^{(\alpha)}(p, t) \equiv V_{13}^{M\dagger} \widetilde{\Psi}^{(\alpha)}(p, t), \quad (2.40)$$

where the orthogonal matrix

$$V_{13}^M \equiv \begin{pmatrix} \cos \vartheta_{13}^M & 0 & \sin \vartheta_{13}^M \\ 0 & 1 & 0 \\ -\sin \vartheta_{13}^M & 0 & \cos \vartheta_{13}^M \end{pmatrix}, \quad (2.41)$$

is defined in such a way that the matrix

$$V_{13}^{M\dagger} \widetilde{M}^2 V_{13}^M \equiv M_M^2 \equiv \text{diag}(m_{M1}^2, 0, m_{M3}^2) \quad (2.42)$$

is diagonal. Then, we obtain that the effective mixing angle in matter ϑ_{13}^M is given by

$$\cos 2\vartheta_{13}^M = \frac{m_3^2 \cos 2\vartheta_{13} - A_{CC}}{\sqrt{(m_3^2 \cos 2\vartheta_{13} - A_{CC})^2 + (m_3^2 \sin 2\vartheta_{13})^2}}. \quad (2.43)$$

If $\cos 2\vartheta_{13} > 0$, for $A_{CC} \gg m_3^2$ the effective mixing angle ϑ_{13}^M for neutrinos is approximately equal to $\pi/2$. The corresponding effective mixing angle for anti-neutrinos, which we will denote as $\bar{\vartheta}_{13}^M$, tends to vanish because \bar{A}_{CC} is negative. When $A_{CC} = m_3^2 \cos 2\vartheta_{13}$ there is a resonance: $\vartheta_{13}^M = \pi/4$ and the mixing in the 1-3 sector is maximal. If $\cos 2\vartheta_{13} < 0$, the resonance condition can be realized for anti-neutrinos ($\bar{\vartheta}_{13}^M = \pi/4$) at $\bar{A}_{CC} = \cos 2\vartheta_{13}$. In this case $\bar{\vartheta}_{13}^M \simeq \pi/2$ and $\vartheta_{13}^M \simeq 0$ for $A_{CC} \gg m_3^2$. However, the analogy with the quark sector, in which there is a hierarchy of mixing that respects the mass hierarchy, suggests that a small value of ϑ_{13} is natural and that the resonance condition can be realized for neutrinos.

The evolution equation for $\Psi_M^{(\alpha)}(p, t)$ is diagonal: multiplying Eq.(2.26) by $V_{13}^{M\dagger}$ on the left, we have

$$i \frac{d}{dt} \Psi_M^{(\alpha)}(p, t) = \frac{M_M^2}{2p} \Psi_M^{(\alpha)}(p, t), \quad (2.44)$$

with $M_M^2 = \text{diag}(m_{M1}^2, 0, m_{M3}^2)$. It is important to notice that the assumption of a constant matter density plays here a crucial role. Indeed, if the matter density were not constant, the effective mixing matrix V_{13}^M would be dependent on t and the time derivative of V_{13}^M would induce additional non-diagonal terms in the evolution equation (2.44).

The explicit evolution equation for the amplitudes $\psi_{Mk}^{(\alpha)}(p, t)$, with $k = 1, 2, 3$, is

$$i \frac{d}{dt} \psi_{Mk}^{(\alpha)}(p, t) = \frac{m_{Mk}^2}{2p} \psi_{Mk}^{(\alpha)}(p, t). \quad (2.45)$$

This equation has the straightforward solution

$$\psi_{Mk}^{(\alpha)}(p, t) = \exp \left[-i \frac{m_{Mk}^2}{2p} (t - t_0) \right] \psi_{Mk}^{(\alpha)}(p, t_0), \quad (2.46)$$

which can be written in a matrix form as

$$\Psi_M^{(\alpha)}(p, t) = \exp \left[-i \frac{M_M^2}{2p} (t - t_0) \right] \Psi_M^{(\alpha)}(p, t_0). \quad (2.47)$$

This equation gives the evolution in time of the amplitudes $\psi_{Mk}^{(\alpha)}(p, t)$. However, we are interested in the evolution in time of the amplitudes $\psi_\beta^{(\alpha)}(p, t)$ whose absolute value squared give the oscillation probabilities through Eq.(2.14). The amplitudes $\psi_\beta^{(\alpha)}(p, t)$ are the elements of $\Psi_W^{(\alpha)}(p, t)$ and, using Eqs.(2.25) and (2.40) we can express $\Psi_W^{(\alpha)}(p, t)$ in terms of $\Psi_M^{(\alpha)}(p, t)$ as

$$\Psi_W^{(\alpha)}(p, t) = V_{23} \tilde{\Psi}^{(\alpha)}(p, t) = V_{23} V_{13}^M \Psi_M^{(\alpha)}(p, t) = V^M \Psi_M^{(\alpha)}(p, t), \quad (2.48)$$

with the orthogonal matrix

$$V^M \equiv V_{23} V_{13}^M = \begin{pmatrix} \cos \vartheta_{13}^M & 0 & \sin \vartheta_{13}^M \\ -\sin \vartheta_{23} \sin \vartheta_{13}^M & \cos \vartheta_{23} & \sin \vartheta_{23} \cos \vartheta_{13}^M \\ -\cos \vartheta_{23} \sin \vartheta_{13}^M & -\sin \vartheta_{23} & \cos \vartheta_{23} \cos \vartheta_{13}^M \end{pmatrix}. \quad (2.49)$$

Notice that the elements of the third column of V^M have the same structure as the elements of the third column of the mixing matrix U (see Eq.(A.20)), in terms of the mixing angle ϑ_{23} and the effective mixing angle in matter ϑ_{13}^M , which replaces the vacuum mixing angle ϑ_{13} . Let us emphasize, however, that the matrix V^M can be considered as

the effective mixing matrix in matter only for the study of the oscillations in matter in the scheme with three neutrinos and the mass hierarchy (1.1). In this case, the approximation $m_1 = m_2 = 0$ implies that there is no mixing in the 1-2 sector and W_{12} is equal to the identity matrix. Notice that the first row of V^M , corresponding to the electron neutrino, is particularly simple, with $V_{e2}^M = 0$, because the electron neutrino feels only the mixing in the 1-3 sector. Physically, the special status of the electron neutrino follows from its direct charged current interaction with the electrons in the medium, represented by the quantity A_{CC} .

Substituting the solution (2.47) for $\Psi_M^{(\alpha)}(p, t)$ and using the orthogonality of V^M , we obtain

$$\Psi_W^{(\alpha)}(p, t) = V^M \exp \left[-i \frac{M_M^2}{2p} (t - t_0) \right] (V^M)^T \Psi_W^{(\alpha)}(p, t_0). \quad (2.50)$$

Explicitly, we have

$$\psi_\beta^{(\alpha)}(p, t) = \sum_{k, \rho} V_{\beta k}^M \exp \left[-i \frac{m_{Mk}^2}{2p} (t - t_0) \right] V_{\rho k}^M \psi_\rho^{(\alpha)}(p, t_0). \quad (2.51)$$

This is the solution of the evolution equation for the amplitudes $\psi_\beta^{(\alpha)}(p, t)$ in a slab of matter with a constant density. In the case of neutrino propagation through a series of slabs of matter with a constant density, as in the interior of the Earth, the solutions (2.51) for confining slabs must be matched in order to have continuity of the flavor amplitudes $\psi_\beta^{(\alpha)}(p, t)$. For example, for a neutrino created at the time t_0 and crossing a series of boundaries between slabs of matter with a constant density at the times t_1, t_2, \dots, t_n , the amplitudes $\psi_\beta^{(\alpha)}(p, t)$ in the $(n+1)^{\text{th}}$ slab are given by the matrix equation

$$\begin{aligned} \Psi_W^{(\alpha)}(p, t) = & \left[V^M e^{-i \frac{M_M^2(t-t_n)}{2p}} (V^M)^T \right]_{(n+1)} \left[V^M e^{-i \frac{M_M^2(t_n-t_{n-1})}{2p}} (V^M)^T \right]_{(n)} \dots \\ & \dots \left[V^M e^{-i \frac{M_M^2(t_2-t_1)}{2p}} (V^M)^T \right]_{(2)} \left[V^M e^{-i \frac{M_M^2(t_1-t_0)}{2p}} (V^M)^T \right]_{(1)} \Psi_W^{(\alpha)}(p, t_0). \end{aligned} \quad (2.52)$$

Here the notation $[\dots]_{(i)}$ indicates that the matter-dependent quantities inside of the square brackets must be evaluated with the matter density of the i^{th} slab. From Eq.(2.14), one can see that the oscillation probabilities are given by the squared moduli of the amplitudes $\psi_\beta^{(\alpha)}(p, t)$ given by Eq.(2.52).

It is clear that for $n > 1$ an analytical calculation of the oscillation probabilities is a rather complicated task and of little interest. Therefore, this calculation is done numerically with a computer.

The calculation for $n = 1$, i.e. for the case of a medium with constant density, can be done analytically. In order to derive the oscillation probabilities, we employ the same method as in vacuum (see Eqs.(2.30)–(2.33b)): using the orthogonality relation

$$\sum_{k=1,2} V_{\beta k}^M V_{\alpha k}^M = \delta_{\alpha\beta} - V_{\beta 3}^M V_{\alpha 3}^M, \quad (2.53)$$

the amplitudes (2.51), with $t_0 = 0$ and $\psi_p^{(\alpha)}(p, 0) = \delta_{\alpha p}$, can be written as

$$\begin{aligned}\psi_\beta^{(\alpha)}(p, t) &= V_{\alpha 1}^M V_{\beta 1}^M \exp\left(-i \frac{m_{M1}^2 t}{2p}\right) + V_{\alpha 2}^M V_{\beta 2}^M + V_{\alpha 3}^M V_{\beta 3}^M \exp\left(-i \frac{m_{M3}^2 t}{2p}\right) \\ &= \exp\left(-i \frac{m_{M1}^2 t}{2p}\right) \left\{ \delta_{\alpha\beta} + V_{\alpha 2}^M V_{\beta 2}^M \left[\exp\left(i \frac{m_{M1}^2 t}{2p}\right) - 1 \right] \right. \\ &\quad \left. + V_{\alpha 3}^M V_{\beta 3}^M \left[\exp\left(-i \frac{\Delta m_{M31}^2 t}{2p}\right) - 1 \right] \right\},\end{aligned}\quad (2.54)$$

with

$$\Delta m_{M31}^2 \equiv m_{M3}^2 - m_{M1}^2 = \sqrt{(m_3^2 \cos 2\vartheta_{13} - A_{CC})^2 + (m_3^2 \sin 2\vartheta_{13})^2}. \quad (2.55)$$

For the transition and survival probabilities we obtain

$$P_{\nu_\alpha \rightarrow \nu_\beta} = A_{\alpha;\beta}^M S_{31}^2 - 4 V_{\alpha 1}^M V_{\beta 1}^M V_{\alpha 2}^M V_{\beta 2}^M S_1^2 - 4 V_{\alpha 2}^M V_{\beta 2}^M V_{\alpha 3}^M V_{\beta 3}^M (S_3^2 - S_{31}^2), \quad (2.56a)$$

$$P_{\nu_\alpha \rightarrow \nu_\alpha} = 1 - B_{\alpha;\alpha}^M S_{31}^2 - 4 (V_{\alpha 1}^M)^2 (V_{\alpha 2}^M)^2 S_1^2 - 4 (V_{\alpha 2}^M)^2 (V_{\alpha 3}^M)^2 (S_3^2 - S_{31}^2), \quad (2.56b)$$

respectively. Here

$$S_1^2 \equiv \sin^2\left(\frac{m_{M1}^2 t}{4p}\right), \quad S_3^2 \equiv \sin^2\left(\frac{m_{M3}^2 t}{4p}\right), \quad S_{31}^2 \equiv \sin^2\left(\frac{\Delta m_{M31}^2 t}{4p}\right), \quad (2.57)$$

and

$$A_{\alpha;\beta}^M = 4 (V_{\alpha 3}^M)^2 (V_{\beta 3}^M)^2, \quad (2.58a)$$

$$B_{\alpha;\alpha}^M = \sum_{\beta \neq \alpha} A_{\alpha;\beta}^M = 4 (V_{\alpha 3}^M)^2 [1 - (V_{\alpha 3}^M)^2] \quad (2.58b)$$

are the classical oscillation amplitudes in matter analogous to the corresponding ones in vacuum, $A_{\alpha;\beta}$ and $B_{\alpha;\alpha}$ (see Eqs.(2.33)). The classical oscillation amplitudes in matter $A_{\alpha;\beta}^M$ and $B_{\alpha;\alpha}^M$ have the same structure as the classical oscillation amplitudes in vacuum $A_{\alpha;\beta}$ and $B_{\alpha;\alpha}$, in terms of the mixing angle ϑ_{23} and the effective mixing angle in matter ϑ_{13}^M , which replaces the vacuum mixing angle ϑ_{13} . Therefore, it is easy to see that in the limit $V_{CC} \rightarrow 0$ only the terms involving $A_{\alpha;\beta}^M \rightarrow A_{\alpha;\beta}$ and $B_{\alpha;\alpha}^M \rightarrow B_{\alpha;\alpha}$ survive in Eqs.(2.56) and the oscillation probabilities reduce to the oscillation probabilities in vacuum (2.32).

It is interesting to notice the following features of the oscillation probabilities (2.56):

1. The oscillation probabilities involving the electron neutrino in the initial and/or final state are particularly simple, because $V_{e2}^M = 0$:

$$P_{\nu_e \rightarrow \nu_e} = 1 - B_{e;e}^M S_{31}^2, \quad P_{\nu_e \rightarrow \nu_\mu} = A_{e;\mu}^M S_{31}^2, \quad (2.59)$$

with

$$B_{e;e}^M = \sin^2 2\vartheta_{13}^M, \quad A_{e;\mu}^M = \sin^2 \vartheta_{23} \sin^2 2\vartheta_{13}^M. \quad (2.60)$$

These oscillation probabilities depend only on one oscillation length,

$$L_{\text{osc}}^{(31)} = \frac{4\pi p}{\Delta m_{M31}^2}. \quad (2.61)$$

In the limit $V_{CC} \rightarrow 0$ we have $L_{\text{osc}}^{(31)} \rightarrow L_{\text{osc}}$, where L_{osc} is the oscillation length in vacuum, given in Eq.(2.34).

2. The oscillation probabilities involving only muon and/or tau neutrinos have a complicated structure, depending on three different oscillation lengths: $L_{\text{osc}}^{(31)}$, $L_{\text{osc}}^{(3)}$ and $L_{\text{osc}}^{(1)}$, with

$$L_{\text{osc}}^{(3)} = \frac{4\pi p}{m_{M3}^2}, \quad L_{\text{osc}}^{(1)} = \frac{4\pi p}{m_{M1}^2}. \quad (2.62)$$

In the limit $V_{CC} \rightarrow 0$, we have that $L_{\text{osc}}^{(31)} \rightarrow L_{\text{osc}}$, $L_{\text{osc}}^{(3)} \rightarrow L_{\text{osc}}$ and $L_{\text{osc}}^{(1)} \rightarrow \infty$.

The survival probability of muon neutrinos is given by

$$P_{\nu_\mu \rightarrow \nu_\mu} = 1 - B_{\mu;\mu}^M S_{31}^2 - \sin^2 2\vartheta_{23} \sin^2 \vartheta_{13}^M S_1^2 - \sin^2 2\vartheta_{23} \cos^2 \vartheta_{13}^M (S_3^2 - S_{31}^2), \quad (2.63)$$

with

$$B_{\mu;\mu}^M = \sin^4 \vartheta_{23} \sin^2 2\vartheta_{13}^M + \sin^2 2\vartheta_{23} \cos^2 \vartheta_{13}^M. \quad (2.64)$$

3. The oscillation probabilities (2.56) are invariant under time reversal: $P_{\nu_\alpha \rightarrow \nu_\beta} = P_{\nu_\beta \rightarrow \nu_\alpha}$. This is due to the fact that the effect of a constant matter density along the neutrino path is T invariant. As a consequence, all the oscillation probabilities can be derived from the three probabilities (2.59) and (2.63) using the conservation of probabilities ($\sum_\beta P_{\nu_\alpha \rightarrow \nu_\beta} = 1$) and the invariance under time reversal ($P_{\nu_\alpha \rightarrow \nu_\beta} = P_{\nu_\beta \rightarrow \nu_\alpha}$).
4. The survival and transition probabilities of neutrinos and anti-neutrinos can be different, because the effective mixing angles ϑ_{13}^M , $\bar{\vartheta}_{13}^M$ and the effective squared-masses $m_{M1,3}^2$, $\bar{m}_{M1,3}^2$ for neutrinos and anti-neutrinos are different ($\bar{A}_{CC} = -A_{CC}$). This is a consequence of the fact that the medium is neither CP invariant nor CPT invariant.

When $A_{CC} \gtrsim m_3^2$, which can be realized with high matter density and neutrino energy, the effective mixing angle ϑ_{13}^M of neutrinos becomes large and approaches $\pi/2$ for $A_{CC} \gg m_3^2$ (see Eq.(2.43); here we assume $\cos 2\vartheta_{13} > 0$). This means that the matter effect is relevant and can dramatically modify the oscillation probabilities. From Eqs.(2.59) and (2.60) we see that, in the case of a medium with constant density, when $A_{CC} \gg m_3^2$ and $\vartheta_{13}^M \simeq \pi/2$ the transition probabilities of electron neutrinos are suppressed. The same suppression is realized for anti-neutrinos, which have $\bar{\vartheta}_{13}^M \simeq 0$. Assuming a small value for ϑ_{13} , the maximum difference between the neutrino and anti-neutrino oscillation probabilities is obtained when the resonance condition $A_{CC} = m_3^2 \cos 2\vartheta_{13}$ is satisfied for neutrinos, which implies that $\vartheta_{13}^M \simeq \pi/4$ for neutrinos, whereas $\bar{\vartheta}_{13}^M < \vartheta_{13}$ for anti-neutrinos. At the resonance the oscillations of the survival probability of electron neutrinos are maximal, $P_{\nu_e \rightarrow \nu_e} = 1 - S_{31}^2$, while the other probabilities depend on the value of ϑ_{23} .

2.2 Low energy neutrinos

It has been pointed out [75, 76] that the matter effect may be not negligible even in the case of low matter density or low neutrino energy⁴, i.e. for $A_{CC} = 2pV_{CC} \ll m_3^2$. In this case, the mass eigenvalues can be approximated by

$$m_{M1}^2 \simeq A_{CC} (1 + \cos 2\vartheta_{13}) / 2, \quad (2.65a)$$

$$m_{M3}^2 \simeq m_3^2 + A_{CC} (1 - \cos 2\vartheta_{13}) / 2, \quad (2.65b)$$

$$\Delta m_{M31}^2 \simeq m_3^2 - A_{CC} \cos 2\vartheta_{13}. \quad (2.65c)$$

It is important to notice [76] that m_{M1}^2 is proportional to A_{CC} , which in turn is proportional to the neutrino energy ($A_{CC} = 2pV_{CC}$). Hence, the phase

$$\frac{m_{M1}^2 t}{2p} \simeq \frac{A_{CC} t}{4p} (1 + \cos 2\vartheta_{13}) = \frac{V_{CC} t}{2} (1 + \cos 2\vartheta_{13}) \quad (2.66)$$

is independent of the neutrino momentum and can be relevant for low-energy atmospheric neutrinos (as those corresponding to the Kamiokande sub-GeV data). The value of the potential V_{CC} is given by

$$\begin{aligned} V_{CC} &= \sqrt{2} G_F N_e = 7.63 \times 10^{-14} \left(\frac{N_e}{N_A \text{cm}^{-3}} \right) \text{eV} \\ &= 3.87 \times 10^{-4} \left(\frac{N_e}{N_A \text{cm}^{-3}} \right) \text{Km}^{-1}, \end{aligned} \quad (2.67)$$

where N_A is the Avogadro number. The interior of the Earth has an electron number density N_e that goes from about $2 N_A \text{cm}^{-3}$ in the mantle to about $6 N_A \text{cm}^{-3}$ in the inner core, with an average value of about $3 N_A \text{cm}^{-3}$ (see Fig.1B). For a propagation of 10^4Km we have $V_{CC}t/2 \simeq 2\pi$, which shows that the phase (2.66) could be relevant for low-energy atmospheric neutrinos.

When $A_{CC} \ll m_3^2$, the oscillation probabilities depend on two oscillation lengths:

$$L_{\text{osc}}^{(31)} \simeq L_{\text{osc}}^{(3)} \simeq \frac{4\pi p}{m_3^2} \equiv L_{\text{osc}}^{\text{short}}, \quad L_{\text{osc}}^{(1)} \simeq \frac{4\pi}{V_{CC} (1 + \cos 2\vartheta_{13})} \equiv L_{\text{osc}}^{\text{long}}. \quad (2.68)$$

The short oscillation length $L_{\text{osc}}^{\text{short}}$ coincides with the oscillation length in vacuum, whereas the long oscillation length $L_{\text{osc}}^{\text{long}}$ is due to the matter effect. For example, for $m_3^2 = 10^{-2} \text{eV}^2$ (which is close to the best fit of the atmospheric neutrino data), $p = 500 \text{MeV}$ (which is in the range of the Kamiokande sub-GeV data), $N_e = 3 N_A \text{cm}^{-3}$, we have $L_{\text{osc}}^{\text{short}} \simeq 10^2 \text{Km}$ and $L_{\text{osc}}^{\text{long}} \simeq 10^4 \text{Km}$. The oscillating terms s_3^2 and s_{31}^2 in Eq.(2.57)

⁴ Let us remind that, as discussed after Eq.(2.29), caution is needed for low-energy neutrinos if $m_2^2 \gtrsim 10^{-5} \text{eV}^2$. In this case the considerations presented in this subsection can be applied only to neutrinos in the momentum range $m_2^2 R_\oplus / 2 \ll p \ll m_3^2 / 2V_{CC}$. For example, for $m_2^2 = 1.5 \times 10^{-5} \text{eV}^2$ (that corresponds to the best-fit point of the large mixing angle MSW solution of the solar neutrino problem [71]), $m_3^2 = 10^{-2} \text{eV}^2$ and $V_{CC} = 5 \times 10^{-13} \text{eV}$ (that corresponds to the density in the core of the earth) we have the momentum range $200 \text{MeV} \ll p \ll 10 \text{GeV}$.

depend on the short oscillation length $L_{\text{osc}}^{\text{short}}$ and oscillate very fast on a distance scale bigger than 10^3 Km. Therefore, one can study the slow oscillations of the probabilities due to $L_{\text{osc}}^{\text{long}}$, averaging the probabilities over the fast oscillations due to $L_{\text{osc}}^{\text{short}}$:

$$\langle P_{\nu_e \rightarrow \nu_e} \rangle = 1 - \frac{1}{2} B_{e;e}^M, \quad \langle P_{\nu_e \rightarrow \nu_\mu} \rangle = \frac{1}{2} A_{e;\mu}^M, \quad (2.69a)$$

$$\langle P_{\nu_\mu \rightarrow \nu_\mu} \rangle = 1 - \frac{1}{2} B_{\mu;\mu}^M - \sin^2 2\vartheta_{23} \sin^2 \vartheta_{13}^M \sin^2 \left(\frac{t}{L_{\text{osc}}^{\text{long}}} \right), \quad (2.69b)$$

with $B_{e;e}^M$, $A_{e;\mu}^M$ and $B_{\mu;\mu}^M$ given by Eqs.(2.60) and (2.64).

One can see that the averaged value of the survival and transition probabilities of electron neutrinos are constant and very close to the corresponding averaged probabilities in vacuum (for $A_{CC} \ll m_3^2$ we have $\vartheta_{13}^M \simeq \vartheta_{13}$, $B_{e;e}^M \simeq B_{e;e}$ and $A_{e;\mu}^M \simeq A_{e;\mu}$),

$$\langle P_{\nu_e \rightarrow \nu_e} \rangle_{\text{vac}} = 1 - \frac{1}{2} B_{e;e}, \quad \langle P_{\nu_e \rightarrow \nu_\mu} \rangle_{\text{vac}} = \frac{1}{2} A_{e;\mu}. \quad (2.70)$$

On the other hand, the averaged value of the survival probability of muon neutrinos has the additional term depending on $L_{\text{osc}}^{\text{long}}$ with respect to the corresponding averaged probability in vacuum

$$\langle P_{\nu_\mu \rightarrow \nu_\mu} \rangle_{\text{vac}} = 1 - \frac{1}{2} B_{\mu;\mu}. \quad (2.71)$$

The behaviour of $\langle P_{\nu_\mu \rightarrow \nu_\mu} \rangle$ as a function of the propagation distance $L = t$ in a medium with a constant electron density $N_e = 3 N_A \text{ cm}^{-3}$ is depicted in Fig.2 for neutrinos and anti-neutrinos and two sets of values of the mixing parameters: (A) $|U_{e3}|^2 = |U_{\mu3}|^2 = 1/3$ (which corresponds to maximal mixing of the three neutrinos) and (B) $|U_{e3}|^2 = 0.3$, $|U_{\mu3}|^2 = 0.5$ (which is close to the best fit of the Kamiokande data; see Eq.(3.6)). The solid lines represent $\langle P_{\nu_\mu \rightarrow \nu_\mu} \rangle$, the dashed lines represent $\langle P_{\bar{\nu}_\mu \rightarrow \bar{\nu}_\mu} \rangle$ and the dotted lines represent the averaged survival probability in vacuum (2.71). From the comparison with the averaged survival probability in vacuum, it is clear that the oscillations in matter can be rather different than in vacuum even if $A_{CC} \ll m_3^2$. One can also see a small difference between the averaged survival probabilities of muon neutrinos and anti-neutrinos, due to the fact that ϑ_{13}^M and $\bar{\vartheta}_{13}^M$ are not exactly equal to ϑ_{13} and different between each other.

In Fig.3A,B we present the behaviour of $\langle P_{\nu_\mu \rightarrow \nu_\mu} \rangle$ and $\langle P_{\bar{\nu}_\mu \rightarrow \bar{\nu}_\mu} \rangle$ for neutrinos propagating in the interior of the Earth as a function of the zenithal angle θ . These figures correspond to the same two sets of values of the mixing parameters as in Fig.2. The values of $\langle P_{\nu_\mu \rightarrow \nu_\mu} \rangle$ (and similarly those of $\langle P_{\bar{\nu}_\mu \rightarrow \bar{\nu}_\mu} \rangle$) are obtained assuming $m_3^2 = 10^{-2} \text{ eV}^2$, $p = 500 \text{ MeV}$ and averaging numerically the probability $P_{\nu_\mu \rightarrow \nu_\mu} = \left| \psi_\mu^{(\mu)}(p, t) \right|^2$, with $\psi_\mu^{(\mu)}(p, t)$ given by Eq.(2.52), over the fast oscillations corresponding to $L_{\text{osc}}^{\text{short}} \simeq 10^2 \text{ Km}$. Figure 3C shows the slant depth as a function of the zenithal angle θ . One can see that the irregularities of $\langle P_{\nu_\mu \rightarrow \nu_\mu} \rangle$ and $\langle P_{\bar{\nu}_\mu \rightarrow \bar{\nu}_\mu} \rangle$ correspond to irregularities of the slant depth, which occur for trajectories that graze the boundaries between the different shells with approximately constant density.

The effect of $L_{\text{osc}}^{\text{long}}$ will be negligible in the long-baseline experiments of the next generation (CHOOZ [31], Palo Verde [32], KEK–SuperKamiokande [33], Fermilab–Soudan [34], CERN–Gran Sasso [35]) because the baseline will be shorter than 10^3 Km. However, it is interesting to notice that $L_{\text{osc}}^{\text{long}}$ is independent from the value of m_3 and is very sensitive to the matter density. Therefore, the observation of the effect of $L_{\text{osc}}^{\text{long}}$ in future very-long-baseline neutrino oscillation experiments could be helpful for a study of a detailed tomography of the interior of the Earth [78].

3 Analysis of the Kamiokande atmospheric neutrino data

In this Section we present our fit of the Kamiokande atmospheric neutrino data in the scheme with mixing of three neutrinos and a mass hierarchy considered in the previous Section. In this scheme the probability $P_{\nu_\alpha \rightarrow \nu_\beta}(E, \cos \theta; m_3^2, |U_{e3}|^2, |U_{\mu 3}|^2)$ of $\nu_\alpha \rightarrow \nu_\beta$ oscillations for a neutrino with energy $E \simeq p$ arriving at the detector from a direction with a zenith angle θ depends on the three parameters $m_3^2, |U_{e3}|^2, |U_{\mu 3}|^2$ and on the matter density along the neutrino trajectory. (In this article, we do not consider preliminary data from the SuperKamiokande experiment, waiting for more refined data to be available in the future.)

3.1 The experimental data

We have analyzed the neutrino-induced e -like and μ -like event rates measured by the Kamiokande [1, 2, 3] experiment.

The Kamiokande data sample is divided into two classes: the low energy sub-GeV data, including only fully contained events, and the high energy multi-GeV data, including both fully and partially contained events. Additional information on these events is provided by their angular distributions, divided in five zenith-angle bins. In our analysis we fit the angular distribution of the e -like and μ -like multi-GeV data and the total number of e -like and μ -like sub-GeV data reported in Ref.[3]. For the sub-GeV data we do not fit the angular distribution because there is a poor correlation between the directions of the neutrino and the produced charged lepton [3].

The Kamiokande collaboration measured the absolute rate of e -like and μ -like events. In order to analyze the muon-electron flavor composition of atmospheric neutrino events they presented also the ratio of ratios $R_{\mu/e} = (\mu/e)_{\text{exp}}/(\mu/e)_{\text{th}}$, where $(\mu/e)_{\text{exp}}$ is the ratio of μ -like and e -like events measured experimentally and $(\mu/e)_{\text{th}}$ is the same ratio calculated theoretically, without neutrino oscillations. The Kamiokande results

$$R_{\mu/e}^{\text{sub-GeV}} = 0.60_{-0.05}^{+0.06} \pm 0.05, \quad (3.1)$$

$$R_{\mu/e}^{\text{multi-GeV}} = 0.57_{-0.07}^{+0.08} \pm 0.07 \quad (3.2)$$

indicate an anomalous flavor composition in the observed atmospheric neutrino flux, in both the sub-GeV and multi-GeV energy ranges.

In our analysis we did not use the ratio of ratios $R_{\mu/e}$, because, according to the arguments discussed in Ref.[77], its non-Gaussian probability distribution might bias the statistical analysis. Therefore, we preferred to study the separate e -like and μ -like event rates, including in our analysis the correlation of their uncertainties.

3.2 Theoretical calculation

The expected numbers of e -like and μ -like events in each angular bin, under the hypothesis of neutrino oscillations, are given by

$$N_{ei} = N_{ei}^{\text{th}} P_{\nu_e \rightarrow \nu_e}^{(i)} + N_{\mu i}^{\text{th}} P_{\nu_\mu \rightarrow \nu_e}^{(i)}, \quad (3.3)$$

$$N_{\mu i} = N_{ei}^{\text{th}} P_{\nu_e \rightarrow \nu_\mu}^{(i)} + N_{\mu i}^{\text{th}} P_{\nu_\mu \rightarrow \nu_\mu}^{(i)}, \quad (3.4)$$

where N_{ei}^{th} and $N_{\mu i}^{\text{th}}$ are, respectively, the number of e -like and μ -like events in the angular bin i calculated theoretically, under the assumption that there are no oscillations, while $P_{\nu_\alpha \rightarrow \nu_\beta}^{(i)}$ is the averaged probability of $\nu_\alpha \rightarrow \nu_\beta$ transitions (with $\alpha, \beta = e, \mu$) in the bin i . The five bins of $\cos \theta$ for the Kamiokande multi-GeV data are centered around $\langle \cos \theta \rangle_{i=1, \dots, 5} = -0.8, -0.4, 0.0, 0.4, 0.8$, which correspond to the average distances $\langle L \rangle_{i=1, \dots, 5} = 10230, 5157, 852, 54, 26$ Km travelled by neutrinos from the production point down to the detector site.

Since the neutrino oscillation probabilities $P_{\nu_\alpha \rightarrow \nu_\beta}$ are functions of the neutrino energy and of the zenith angle, in order to compare the theoretical calculation with the experimental data, they must be averaged both on the neutrino energy spectrum (different for e -like and μ -like events) and on the angular width of each zenith-angle bin used in our analysis.

Therefore, a preliminary step in our calculations consisted of the evaluation of the averaged probabilities $P_{\nu_\alpha \rightarrow \nu_\beta}^{(i)}(m_3^2, |U_{e3}|^2, |U_{\mu 3}|^2)$ in each angular bin i , for a fixed set of values of the three oscillation parameters $m_3^2, |U_{e3}|^2, |U_{\mu 3}|^2$, defined by the double-integrals

$$P_{\nu_\alpha \rightarrow \nu_\beta}^{(i)}(m_3^2, |U_{e3}|^2, |U_{\mu 3}|^2) = \int d\cos \theta \int dE S_{\nu_\alpha}(E) P_{\nu_\alpha \rightarrow \nu_\beta}(E, \cos \theta; m_3^2, |U_{e3}|^2, |U_{\mu 3}|^2), \quad (3.5)$$

where θ is the zenith angle, E is the neutrino energy and $S_{\nu_\alpha}(E)$ is the energy spectrum of the parent neutrino (with flavor α). These energy spectra were extracted from the figures published in the Ref.[2] for the Kamiokande sub-GeV data and in Ref.[3] for the Kamiokande multi-GeV data.

When matter effects are included in the calculations, the probabilities $P_{\nu_\alpha \rightarrow \nu_\beta}(E, \cos \theta; m_3^2, |U_{e3}|^2, |U_{\mu 3}|^2)$ are not simple functions of the neutrino energy and zenith-angle, but must be calculated numerically by taking into account the matter density along the neutrino path in the Earth. The density and composition of the interior of the Earth is known from seismological measurements (see Refs.[69, 70]). The electron number density N_e varies in a discontinuous way from $1.6 N_A \text{ cm}^{-3}$ near the surface to $6.2 N_A \text{ cm}^{-3}$ in the inner core. However, it is possible to approximate the electron number density profile with a step-like function, each step representing a shell with constant

density (see also Refs.[23]). We approximated the numerical data in Ref.[70] with five shells of constant density (see Fig.1) and we considered the atmosphere as an outer shell with a thickness of 20 Km. The effective neutrino path in each of the shells depends upon the zenith angle of the neutrino trajectory.

The amplitude of $\nu_\alpha \rightarrow \nu_\beta$ transitions for a neutrino with energy $E \simeq p$ in a medium with constant density is given by Eq.(2.51). In the case of a neutrino crossing various shells of different density, the matrices describing the propagation across different shells must be multiplied serially, as in Eq.(2.52), in order to get the amplitude of the transition along the total path. The square modulus of this amplitude gives the probability of $\nu_\alpha \rightarrow \nu_\beta$ oscillations (see Eq.(2.14)). This probability must be folded with the relevant neutrino energy spectrum and integrated over the selected intervals of energy and $\cos \theta$ (see Eq.(3.5)).

We took the values of N_{ei}^{th} and $N_{\mu i}^{\text{th}}$ given by Table 2 (flux A) of Ref.[3] for the Kamiokande sub-GeV data and by Fig.3 of Ref.[3] for the Kamiokande multi-GeV data. The estimated uncertainties of the absolute value of N_{ei}^{th} and $N_{\mu i}^{\text{th}}$ amount to 30%, mainly due to the uncertainties of the value of the calculated electron and muon neutrino fluxes. The estimated relative errors for the ratios $N_{\mu i}^{\text{th}}/N_{ei}^{\text{th}}$ ratio are much smaller: 9% for the Kamiokande sub-GeV data and 12% for the Kamiokande multi-GeV data. In our calculations we neglected the fact that not all e -like and μ -like events are produced by ν_e ($\bar{\nu}_e$) and ν_μ ($\bar{\nu}_\mu$) interactions, respectively. The purity of the e -like and μ -like events is estimated by the Kamiokande Collaboration to be higher than 90% [3].

3.3 Results of the fit

The number of e -like and μ -like events was calculated using the formulas (3.3) and (3.4) for a grid of values of the parameters m_3^2 , $|U_{e3}|^2$, $|U_{\mu 3}|^2$, averaging over the contributions of neutrinos and anti-neutrinos. These values were used together with the experimental results to build a proper χ^2 function. The best fit of the Kamiokande data was obtained for

$$m_3^2 = 2.5 \times 10^{-2} \text{ eV}^2, \quad |U_{e3}|^2 = 0.26, \quad |U_{\mu 3}|^2 = 0.49, \quad (3.6)$$

with $\chi^2 = 6.9$ for 9 degrees of freedom, corresponding to a CL of 65%.

The regions allowed at 90% CL by the Kamiokande data in the $B_{e;e}-m_3^2$, $B_{\mu;\mu}-m_3^2$, $A_{\mu;e}-m_3^2$ and $A_{\mu;\tau}-m_3^2$ planes are presented in Figs.4, 5, 6 and 7, respectively (shadowed regions). Since the oscillation probabilities in vacuum (2.32) have the same form as the corresponding ones in the case of two-neutrino mixing (see Eqs.(2.36)), the allowed regions in the $B_{e;e}-m_3^2$, $B_{\mu;\mu}-m_3^2$, $A_{\mu;e}-m_3^2$ and $A_{\mu;\tau}-m_3^2$ planes can be compared directly with the exclusion plots of the terrestrial reactor and accelerator neutrino oscillation experiments whose data have been analyzed by the experimental collaborations under the assumption of two-generation mixing. This is simply done through the identification of the appropriate $A_{\alpha;\beta}$ or $B_{\alpha;\alpha}$ with $\sin^2 2\vartheta$ and the identification of Δm^2 with m_3^2 . Moreover, the expected sensitivities of future long-baseline experiments are also presented by the experimental collaborations as curves in the $\sin^2 2\vartheta-\Delta m^2$ plane relative

to two-neutrino oscillations in vacuum. Therefore, each of these sensitivity curves can be compared directly with the corresponding allowed region in one of the $A_{\alpha;\beta}-m_3^2$ or $B_{\alpha;\alpha}-m_3^2$ planes. The same reasoning applies to the future results of reactor long-baseline experiments [31, 32], whose neutrino beams propagate in vacuum. On the other hand, the neutrino beams of accelerator long-baseline experiments [33, 34, 35] will propagate in the Earth and matter effects may be significant. Since the effects of matter are different in the cases of two-neutrino and three-neutrino mixing, in order to get information on the mixing parameters in the scheme with three neutrinos with a mass hierarchy considered here it will be necessary to analyze the data with the formalism presented in Section 2⁵.

The dashed and dotted curves in Fig.4 represent, respectively, the exclusion curves obtained in the Bugey [60] and Krasnoyarsk [61] reactor $\bar{\nu}_e$ disappearance experiment (the excluded region lie on the right of the curves). One can see that a part of the shadowed region allowed by the Kamiokande data in the $B_{e;e}-m_3^2$ plane is excluded by the results of the reactor neutrino oscillation experiments (the lightly shadowed region). Only the darkly shadowed region in Fig.4 is allowed by the results of the Kamiokande and reactor experiments. In Fig.4 we have also plotted the sensitivity curves of the CHOOZ [31] and Palo Verde [32] long-baseline $\bar{\nu}_e$ disappearance experiments with reactor anti-neutrinos (the dash-dotted and dash-dot-dotted curves). One can see that a large part of the allowed region will be explored by the CHOOZ and Palo Verde experiments.

The region allowed by the Kamiokande data in the $B_{\mu;\mu}-m_3^2$ plane, shown in Fig.5, is not constrained by the results of terrestrial neutrino oscillation experiments. Indeed, the best limit at small values of Δm^2 is provided by the CDHS [79] $\bar{\nu}_\mu$ disappearance experiment, whose exclusion curve lies rather far from the Kamiokande-allowed region, as shown in Fig.5 (the dashed curve). In Fig.4 we have also plotted the sensitivity curves of the K2K [33] and MINOS [34] long-baseline experiments (the dash-dotted and dash-dot-dotted curves), which show that the Kamiokande-allowed region will be explored in the near future.

A part of the shadowed region allowed by the Kamiokande data in the $A_{\mu;e}-m_3^2$ plane, shown in Fig.6, is excluded by the results of the reactor neutrino oscillation experiments (the lightly shadowed region), leaving the darkly shadowed region allowed by the results of the Kamiokande and reactor experiments. As shown in Fig.6, most of this allowed region will be explored by the K2K, MINOS and ICARUS [35] long-baseline experiments, whose sensitivity curves are represented by the long-dashed, dash-dotted and dash-dot-dotted curves, respectively.

Finally, Fig.7 shows the Kamiokande-allowed region in the $A_{\mu;\tau}-m_3^2$ plane, part of which is indirectly excluded by the results of the reactor neutrino oscillation experiments (the lightly shadowed region). Indeed, in the lightly shadowed region the amplitude $A_{\nu_\mu;\nu_\tau}$ is rather small and the fit of the Kamiokande data requires large values of the amplitude $A_{\nu_\mu;\nu_e}$, which, because of the inequality $A_{\nu_\mu;\nu_e} \leq B_{\nu_e;\nu_e}$, lie in the region excluded by

⁵ Let us notice that, since the energy of accelerator neutrinos in long-baseline experiments is of the order of 10 GeV, the formalism presented in Section 2 can be applied without caveats also in the case of the large mixing angle solution [48, 71] of the solar neutrino problem, for which $m_2^2 \lesssim 3 \times 10^{-5} \text{ eV}^2$ and $m_2^2 R_\oplus / 2p \lesssim 5 \times 10^{-2}$.

the results of the Bugey and Krasnoyarsk reactor experiments. Hence, only the darkly shadowed region is allowed by the results of the Kamiokande and reactor experiments. As shown in Fig.7, this region will be explored by the MINOS and ICARUS long-baseline experiments, whose sensitivity curves are represented by the dash-dotted and dash-dot-dotted curves, respectively. Since the allowed region extends at large values of $A_{\nu_\mu; \nu_\tau}$, the Kamiokande data indicate that $\nu_\mu \rightarrow \nu_\tau$ oscillations could be observed with a large statistics by the MINOS and ICARUS experiments.

The results of our analysis are similar to those presented in Ref.[24], where the same scheme with three neutrinos and the mass hierarchy (1.1) was used, but matter effects were not taken into account. However, one must notice that the presence of matter is important because it modifies the phases of neutrino oscillations [75] and its effect is to slightly enlarge the allowed region of the mixing parameters towards low values of m_3^2 .

4 Conclusions

We have presented a comprehensive formalism for the description of neutrino oscillations in the Earth in the case with three massive neutrinos whose masses satisfy the hierarchical pattern (1.1). Such a scheme is allowed by the see-saw mechanism for the generation of neutrino masses and permits one to explain the solar and atmospheric neutrino problems through neutrino oscillations if $m_2^2 \sim 10^{-5}$ or 10^{-10} eV² and $m_3^2 \sim 10^{-2}$ eV².

In Section 2.2 we have discussed the matter effect on the oscillations of neutrinos with low energy and have shown that the oscillation probabilities depend on two oscillation lengths: $L_{\text{osc}}^{\text{short}}$ which is the same as the oscillation length in vacuum and $L_{\text{osc}}^{\text{long}} \sim 10^4$ Km (see Eq.(2.68)). The oscillation length $L_{\text{osc}}^{\text{long}}$ is independent of the value of the mass m_3 of the heavy neutrino and the neutrino energy, and is very sensitive to the matter density. Future very-long-baseline neutrino oscillation experiments could observe the oscillations due to $L_{\text{osc}}^{\text{long}}$, after averaging the oscillation probabilities over the fast oscillations due to $L_{\text{osc}}^{\text{short}}$. The sensitivity of these averaged oscillations to the matter density along the neutrino path could allow one to obtain a detailed tomography of the interior of the Earth.

In Section 3 we discussed the analysis of the Kamiokande atmospheric data and presented our results in the form of allowed regions in the $B_{e;e}-m_3^2$, $B_{\mu;\mu}-m_3^2$, $A_{\mu;e}-m_3^2$ and $A_{\mu;\tau}-m_3^2$ planes (see Figs.4, 5, 6 and 7). The knowledge of the allowed regions in these planes is useful because the oscillation probabilities in vacuum (2.32) in the scheme under consideration have the same form as the oscillation probabilities in vacuum (2.36) in the case of two-neutrino mixing, which have been used by the experimental collaborations in the analysis of the data of terrestrial oscillation experiments with reactor and accelerator neutrinos, yielding exclusion curves in the $\sin^2 2\vartheta-\Delta m^2$ plane. Identifying the appropriate $A_{\alpha;\beta}$ or $B_{\alpha;\alpha}$ with $\sin^2 2\vartheta$ and m_3^2 with Δm^2 , the exclusion curves in the $\sin^2 2\vartheta-\Delta m^2$ plane obtained by the terrestrial neutrino oscillation experiments can be plotted directly in the $B_{e;e}-m_3^2$, $B_{\mu;\mu}-m_3^2$, $A_{\mu;e}-m_3^2$ and $A_{\mu;\tau}-m_3^2$ planes and can be compared directly with the regions allowed by the analysis of the Kamiokande data. The same reasoning applies to the sensitivity curves and future results of long-baseline experiments evaluated under

the assumption of two-neutrino oscillations in vacuum.

Our analysis of the Kamiokande data took into account the presence of matter in the oscillations of neutrinos passing through the Earth, whose effect is to slightly enlarge the allowed region towards low values of m_3^2 . The best fit is obtained for $m_3^2 = 2.5 \times 10^{-2} \text{ eV}^2$ and from Figs.4, 5, 6 and 7 one can see that the allowed region of m_3^2 extends from about $3.5 \times 10^{-3} \text{ eV}^2$ to about $3.5 \times 10^{-2} \text{ eV}^2$.

From Figs.4, 5, 6 and 7 one can see that the long-baseline experiments with reactor (CHOOZ and Palo Verde) and accelerator (K2K, MINOS and ICARUS) neutrinos could observe neutrino oscillations in all channels with a relatively large statistics⁶.

The region in the $A_{\mu;\tau}-m_3^2$ plane allowed by the results of the Kamiokande and reactor neutrino oscillation experiments extends at large values of $A_{\nu_\mu;\nu_\tau}$ (see Fig.7). Hence, the Kamiokande data indicate that the MINOS and ICARUS long-baseline experiments could observe a relatively large signal in the channel $\nu_\mu \rightarrow \nu_\tau$. This could be the first direct observation of the tau neutrino.

Acknowledgments

We would like to thank J. Pantaleone for his suggestion of the effect discussed in Section 2.2.

A The mixing matrix

A 3×3 unitary matrix U can be written as (see Refs.[80, 63])

$$U = D(\omega) \prod_{a < b} W_{ab}(\vartheta_{ab} e^{i\eta_{ab}}) \quad (a, b = 1, 2, 3), \quad (\text{A.1})$$

with the unitary matrices

$$D(\omega) = \text{diag}(e^{i\omega_1}, e^{i\omega_2}, e^{i\omega_3}), \quad (\text{A.2})$$

$$\begin{aligned} [W_{ab}(\vartheta_{ab} e^{i\eta_{ab}})]_{rs} = & \delta_{rs} + (\cos \vartheta_{ab} - 1) (\delta_{ra} \delta_{sa} + \delta_{rb} \delta_{sb}) \\ & + \sin \vartheta_{ab} (e^{i\eta_{ab}} \delta_{ra} \delta_{sb} - e^{-i\eta_{ab}} \delta_{rb} \delta_{sa}). \end{aligned} \quad (\text{A.3})$$

⁶After we finished this work the CHOOZ collaboration disclosed its first results (M. Apollonio *et al.*, Phys. Lett. B **420**, 397 (1998)), which are compatible with the hypothesis of absence of $\bar{\nu}_e$ oscillations and lead to the upper bound $\sin^2 2\vartheta \lesssim 0.18$ for $\Delta m^2 \gtrsim 10^{-3} \text{ eV}^2$ at 90% CL. This limit is close to the CHOOZ sensitivity curve shown in Fig.4 and implies that large $\nu_\mu \leftrightarrow \nu_e$ oscillations of atmospheric neutrinos are excluded. However, a subdominant contribution from $\nu_\mu \leftrightarrow \nu_e$ oscillations to the atmospheric neutrino anomaly remains an interesting possibility (see also G.L. Fogli, E. Lisi, A. Marrone and D. Montanino, hep-ph/9711421).

Here $D(\omega)$ is a diagonal matrix depending from the set of phases $\omega = (\omega_1, \omega_2, \omega_3)$ and the matrices $W_{ab}(\vartheta_{ab}e^{i\eta_{ab}})$ are unitary and unimodular. For example, we have

$$W_{12}(\vartheta_{12}e^{i\eta_{12}}) = \begin{pmatrix} \cos \vartheta_{12} & \sin \vartheta_{12} e^{i\eta_{12}} & 0 \\ -\sin \vartheta_{12} e^{-i\eta_{12}} & \cos \vartheta_{12} & 0 \\ 0 & 0 & 1 \end{pmatrix}. \quad (\text{A.4})$$

The matrices $D(\lambda)$ and $W_{ab}(\vartheta_{ab}e^{i\eta_{ab}})$ satisfy the useful identity

$$D(\lambda) W_{ab}(\vartheta_{ab}e^{i\eta_{ab}}) D(\lambda)^\dagger = W_{ab}(\vartheta_{ab}e^{i(\lambda_a + \eta_{ab} - \lambda_b)}) , \quad (\text{A.5})$$

for any set of phases $\lambda = (\lambda_1, \lambda_2, \lambda_3)$. Using the identity (A.5) it is clear that the matrix $W_{ab}(\vartheta_{ab}e^{i\eta_{ab}})$ can be written as

$$W_{ab}(\vartheta_{ab}e^{i\eta_{ab}}) = D_{ab} V_{ab} D_{ab}^\dagger , \quad (\text{A.6})$$

with

$$[D_{ab}]_{rs} = \delta_{rs} + (e^{i\eta_{ab}} - 1) \delta_{ra} \delta_{sa} , \quad (\text{A.7})$$

$$[V_{ab}]_{rs} = \delta_{rs} + (\cos \vartheta_{ab} - 1) (\delta_{ra} \delta_{sa} + \delta_{rb} \delta_{sb}) + \sin \vartheta_{ab} (\delta_{ra} \delta_{sb} - \delta_{rb} \delta_{sa}) . \quad (\text{A.8})$$

The matrix V_{ab} operates a rotation of an angle ϑ_{ab} in the $\nu_a - \nu_b$ plane. For example, we have

$$V_{12} = \begin{pmatrix} \cos \vartheta_{12} & \sin \vartheta_{12} & 0 \\ -\sin \vartheta_{12} & \cos \vartheta_{12} & 0 \\ 0 & 0 & 1 \end{pmatrix} , \quad D_{12} = \begin{pmatrix} e^{i\eta_{12}} & 0 & 0 \\ 0 & 1 & 0 \\ 0 & 0 & 1 \end{pmatrix} . \quad (\text{A.9})$$

The expression (A.1) for U can be written as

$$U = D(\omega - \lambda) \left(\prod_{a < b} D(\lambda) W_{ab}(\vartheta_{ab}e^{i\eta_{ab}}) D(\lambda)^\dagger \right) D(\lambda) , \quad (\text{A.10})$$

with the set of arbitrary phases $\lambda = (\lambda_1, \lambda_2, \lambda_3)$. Using the identity (A.5), we have

$$U = D(\omega - \lambda) \left(\prod_{a < b} W_{ab}(\vartheta_{ab}e^{i(\lambda_a + \eta_{ab} - \lambda_b)}) \right) D(\lambda) . \quad (\text{A.11})$$

The set of arbitrary phases $\lambda = (\lambda_1, \lambda_2, \lambda_3)$ can be chosen in order to extract two of the three phases η_{ab} from the corresponding W_{ab} . Only two phases η_{ab} can be extracted because there are only two independent differences $\lambda_a - \lambda_b$. For example, one can extract η_{13} and η_{23} with the choice

$$\lambda_1 - \lambda_3 = -\eta_{13} , \quad \lambda_2 - \lambda_3 = -\eta_{23} . \quad (\text{A.12})$$

Then, η_{12} cannot be extracted because $\lambda_1 - \lambda_2 = -\eta_{13} + \eta_{23}$ is no longer arbitrary.

The order of the product of the unitary matrices W_{ab} in Eq.(A.1) is arbitrary. Making the choice (A.12) and $\lambda_3 = 0$, the mixing matrix can be written as

$$U = D(\omega - \lambda) V_{23} V_{13} W_{12} D(\lambda). \quad (\text{A.13})$$

with

$$D(\omega - \lambda) = \text{diag}(e^{i(\omega_1 + \eta_{13})}, e^{i(\omega_2 + \eta_{23})}, e^{i\omega_3}), \quad (\text{A.14})$$

$$W_{12} \equiv W_{12}(\vartheta_{12} e^{i\eta_{12}}) = D_{12} V_{12} D_{12}^\dagger, \quad (\text{A.15})$$

$$D(\lambda) = \text{diag}(e^{-i\eta_{13}}, e^{-i\eta_{23}}, 1). \quad (\text{A.16})$$

The mixing matrix U appears in the lepton charged-current (the charged lepton fields are defined as mass eigenstates, because they are observed in the experiments, whereas neutrinos are never observed directly)

$$\begin{aligned} j^\mu &= 2 \sum_{\alpha=e,\mu,\tau} \ell_{\alpha L} \gamma^\mu \nu_{\alpha L} = 2 \sum_{\alpha=e,\mu,\tau} \sum_{k=1,2,3} \ell_{\alpha L} \gamma^\mu U_{\alpha k} \nu_{k L} \\ &= 2 \sum_{\alpha,k} \ell_{\alpha L} \gamma^\mu [D(\omega - \lambda) V_{23} V_{13} W_{12} D(\lambda)]_{\alpha k} \nu_{k L}, \end{aligned} \quad (\text{A.17})$$

where $\ell_{\alpha L}$ represents the left-handed component of the charged lepton field ℓ_α (with $\alpha = e, \mu, \tau$). The three phases in $D(\omega - \lambda)$ can be eliminated with a redefinition of the arbitrary phases of the charged lepton fields, $\ell_\alpha \rightarrow \ell_\alpha e^{-i(\omega_\alpha - \lambda_\alpha)}$, which leads to

$$j^\mu = 2 \sum_{\alpha,k} \ell_{\alpha L} \gamma^\mu [V_{23} V_{13} W_{12} D(\lambda)]_{\alpha k} \nu_{k L}. \quad (\text{A.18})$$

If neutrinos are Dirac particles, also the phases of the neutrino fields are arbitrary and the two phases in $D(\lambda)$ can be eliminated with the redefinition $\nu_k \rightarrow e^{-i\lambda_k} \nu_k$. In the case of Majorana neutrinos the elimination of the two phases contained in $D(\lambda)$ (called in this case ‘‘Majorana phases’’) is not possible, because the Majorana mass term is not invariant under rephasing of the neutrino fields⁷. However, the presence of the Majorana phases does not have any effect on neutrino oscillations [64, 66, 67] (see Eq.(2.23)). In conclusion, the general expression for the mixing matrix can be written as

$$U = V_{23} V_{13} W_{12} D(\lambda). \quad (\text{A.19})$$

Explicitly we have

$$U = \begin{pmatrix} c_{12}c_{13}e^{i\lambda_1} & s_{12}c_{13}e^{i(\eta_{12}+\lambda_2)} & s_{13} \\ -s_{12}c_{23}e^{-i(\eta_{12}-\lambda_1)} - c_{12}s_{23}s_{13}e^{i\lambda_1} & c_{12}c_{23}e^{i\lambda_2} - s_{12}s_{23}s_{13}e^{i(\eta_{12}+\lambda_2)} & s_{23}c_{13} \\ s_{12}s_{23}e^{-i(\eta_{12}-\lambda_1)} - c_{12}c_{23}s_{13}e^{i\lambda_1} & -c_{12}s_{23}e^{i\lambda_2} - s_{12}c_{23}s_{13}e^{i(\eta_{12}+\lambda_2)} & c_{23}c_{13} \end{pmatrix}, \quad (\text{A.20})$$

⁷ For instance, the Majorana mass term for one left-handed neutrino field ν_L is proportional to $\overline{\nu_L} \nu_L^c + \nu_L^c \nu_L = -\nu_L^\dagger \mathcal{C} \nu_L^* - \nu_L^T \mathcal{C}^\dagger \nu_L$, where $\nu_L^c = \mathcal{C} \overline{\nu_L}^T$ and \mathcal{C} is the charge conjugation matrix. It is clear that the Majorana mass term is not invariant under the rephasing $\nu \rightarrow e^{-i\lambda} \nu$.

with $c_{ij} \equiv \cos \vartheta_{ij}$ and $s_{ij} \equiv \sin \vartheta_{ij}$. This parameterization of the mixing matrix is useful for the study of neutrino oscillations in matter (see Section 2).

References

- [1] K.S. Hirata *et al.*, Phys. Lett. B **205**, 416 (1988).
- [2] K.S. Hirata *et al.*, Phys. Lett. B **280**, 146 (1992).
- [3] Y. Fukuda *et al.*, Phys. Lett. B **335**, 237 (1994).
- [4] D. Casper *et al.*, Phys. Rev. Lett. **66**, 2561 (1991); R. Becker-Szendy *et al.*, Phys. Rev. D **46**, 3720 (1992); Nucl. Phys. B (Proc. Suppl.) **38**, 331 (1995).
- [5] T. Kafka, Nucl. Phys. B (Proc. Suppl.) **35**, 427 (1994); M. Goodman, *ibid.* **38**, 337 (1995); W.W.M. Allison *et al.*, Phys. Lett. B **391**, 491 (1997).
- [6] B. Pontecorvo, J. Exptl. Theoret. Phys. **33**, 549 (1957) [Sov. Phys. JETP **6**, 429 (1958)]; J. Exptl. Theoret. Phys. **34**, 247 (1958) [Sov. Phys. JETP **7**, 172 (1958)].
- [7] S.M. Bilenky and B. Pontecorvo, Phys. Rep. **41**, 225 (1978).
- [8] S.M. Bilenky and S.T. Petcov, Rev. Mod. Phys. **59**, 671 (1987).
- [9] R.N. Mohapatra and P.B. Pal, *Massive Neutrinos in Physics and Astrophysics*, World Scientific Lecture Notes in Physics, Vol.41 (World Scientific, Singapore, 1991).
- [10] C.W. Kim and A. Pevsner, *Neutrinos in Physics and Astrophysics*, Contemporary Concepts in Physics, Vol.8 (Harwood Academic Press, Chur, Switzerland, 1993).
- [11] G. Gelmini and E. Roulet, Rept. Prog. Phys. **58**, 1207 (1995).
- [12] S.M. Barr, T.K. Gaisser, P. Lipari and S. Tilav, Phys. Lett. B **214**, 147 (1988); G. Barr, T.K. Gaisser and T. Stanev, Phys. Rev. D **39**, 3532 (1989); W. Frati, T.K. Gaisser, A.K. Mann and T. Stanev, Phys. Rev. D **48**, 1140 (1993); T.K. Gaisser, Nucl. Phys. B (Proc. Suppl.) **35**, 209 (1994).
- [13] T.K. Gaisser, *Cosmic Rays and Particle Physics* (Cambridge University Press, 1990).
- [14] E.V. Bugaev and V.A. Naumov, Yad. Fiz. **45**, 1380 (1987) [Sov. J. Nucl. Phys. **45**, 857 (1987)]; Phys. Lett. B **232**, 391 (1989).
- [15] M. Honda *et al.*, Phys. Lett. B **248**, 193 (1990); Phys. Rev. D **52**, 4985 (1995).
- [16] D.H. Perkins, Astropart. Phys. **2**, 249 (1994).
- [17] K. Martens, Talk presented at the *International Europhysics Conference on High Energy Physics*, 19-26 August 1997, Jerusalem, Israel (<http://www.cern.ch/hep97/-abstract/tpa10.htm>); E. Kearns, Talk presented at the Conference on *Solar Neutrinos: News About SNU's*, 2-6 December 1997, Santa Barbara, California (<http://doug-pc.itp.ucsb.edu/online/snu/>).

- [18] O.G. Ryazhskaya, JETP Lett. **60**, 617 (1994); *ibid.* **61**, 237 (1995).
- [19] Y. Fukuda *et al.*, Phys. Lett. B **388**, 397 (1996).
- [20] C. Berger *et al.*, Phys. Lett. B **227**, 489 (1989); *ibid.* **245**, 305 (1990); K. Daum *et al.*, Z. Phys. C **66**, 417 (1995).
- [21] M. Aglietta *et al.*, Europhys. Lett. **8**, 611 (1989); *ibid.* **15**, 559 (1991).
- [22] R. Clark *et al.*, Phys. Rev. Lett. **79**, 345 (1997).
- [23] G.L. Fogli, E. Lisi and D. Montanino, Phys. Rev. D **49**, 3626 (1994); Astrop. Phys. **4**, 177 (1995), G.L. Fogli, E. Lisi, D. Montanino and G. Scioscia, Phys. Rev. D **55**, 4385 (1997).
- [24] S.M. Bilenky, C. Giunti and C.W. Kim, Astrop. Phys. **4**, 241 (1996).
- [25] M. Mori *et al.*, Phys. Lett. B **270**, 89 (1991).
- [26] R. Becker-Szendy *et al.*, Phys. Rev. Lett. **69**, 1010 (1992).
- [27] M.M. Boliev *et al.*, *Proc. of the 3th International Workshop on Neutrino Telescopes*, Venezia, March 1991.
- [28] MACRO Coll., S. Ahlen *et al.*, Phys. Lett. B **357**, 481 (1995); A. Surdo, Talk presented at the XVIth *International Workshop on Weak Interactions and Neutrinos*, Capri, Italy, 22–28 June 1997; MACRO Coll., M. Ambrosio *et al.*, preprint INFN/AE-97/21.
- [29] W. Frati *et al.*, Phys. Rev. D **48**, 1140 (1993); V. Agrawal *et al.*, *ibid.* **53**, 1314 (1996); T.K. Gaisser *et al.*, *ibid.* **54**, 5578 (1996).
- [30] G.L. Fogli, E. Lisi and A. Marrone, Phys. Rev. D **57**, 5893 (1998).
- [31] C. Bemporad, Proc. of *Neutrino 96*, Helsinki, Finland, 13–19 June 1996, edited by K. Enqvist, K. Huitu and J. Maalampi (World Scientific, Singapore, 1997), p.242; <http://duphy4.physics.drexel.edu/chooz-pub/index.htmlx>.
- [32] F. Boehm *et al.*, *The Palo Verde experiment*, 1996 (<http://www.cco.caltech.edu/~songhoon/Palo-Verde/Palo-Verde.html>); G. Gratta, Proc. of *Neutrino 96*, Helsinki, Finland, 13–19 June 1996, edited by K. Enqvist, K. Huitu and J. Maalampi (World Scientific, Singapore, 1997), p.248.
- [33] Y. Suzuki, Proc. of *Neutrino 96*, Helsinki, Finland, 13–19 June 1996, edited by K. Enqvist, K. Huitu and J. Maalampi (World Scientific, Singapore, 1997), p.237; <http://pnahep.kek.jp/>.

- [34] MINOS Coll., D. Ayres *et al.*, NUMI-L-63, February 1995; S.G. Wojcicki, Proc. of *Neutrino 96*, Helsinki, Finland, 13–19 June 1996, edited by K. Enqvist, K. Huitu and J. Maalampi (World Scientific, Singapore, 1997), p.231; <http://www.hep.anl.gov/-NDK/HyperText/numi.html>.
- [35] ICARUS Coll., P. Cennini *et al.*, LNGS-94/99-I, May 1994; <http://www.aquila.infn.it/icarus/>.
- [36] M. Gell-Mann, P. Ramond, and R. Slansky, in *Supergravity*, ed. F. van Nieuwenhuizen and D. Freedman (North Holland, Amsterdam, 1979), p.315; T. Yanagida, *Proc. of the Workshop on Unified Theory and the Baryon Number of the Universe*, KEK, Japan, 1979; S. Weinberg, Phys. Rev. Lett. **43**, 1566 (1979).
- [37] B.T. Cleveland *et al.*, Nucl. Phys. B (Proc. Suppl.) **38**, 47 (1995).
- [38] K.S. Hirata *et al.*, Phys. Rev. Lett. **65**, 1297 (1990); Phys. Rev. D **44**, 2241 (1991).
- [39] GALLEX Coll., Phys. Lett. B **285**, 376 (1992); *ibid.* **314**, 445 (1993); *ibid.* **327**, 377 (1994); *ibid.* **342**, 440 (1995); *ibid.* **388**, 384 (1996).
- [40] J.N. Abdurashitov *et al.*, Phys. Lett. B **328**, 234 (1994); Phys. Rev. Lett. **77**, 4708 (1996).
- [41] K. Inoue, Talk presented at *TAUP97*, September 7-11, 1997, Laboratori Nazionali del Gran Sasso, Assergi (Italy); R. Svoboda, Talk presented at the Conference on *Solar Neutrinos: News About SNU's*, 2–6 December 1997, Santa Barbara, California (<http://doug-pc.itp.ucsb.edu/online/snu/>).
- [42] J.N. Bahcall and R. Ulrich, Rev. Mod. Phys. **60**, 297 (1988); J.N. Bahcall, *Neutrino Physics and Astrophysics* (Cambridge University Press, 1989); J.N. Bahcall and M.H. Pinsonneault, Rev. Mod. Phys. **64**, 885 (1992); J.N. Bahcall and M.H. Pinsonneault, *ibid.* **67**, 781 (1995);
- [43] S. Turck-Chièze, S. Cahen, M. Cassé and C. Doom, Astrophys. J. **335**, 415 (1988); S. Turck-Chièze and I. Lopes, *ibid.* **408**, 347 (1993); S. Turck-Chièze *et al.*, Phys. Rep. **230**, 57 (1993).
- [44] V. Castellani, S. Degl’Innocenti and G. Fiorentini, Astron. Astrophys. **271**, 601 (1993); S. Degl’Innocenti, Univ. of Ferrara preprint INFN-FE-07-93; V. Castellani *et al.*, Phys. Rep. **281**, 309 (1997).
- [45] A. Dar and G. Shaviv, Nucl. Phys. B (Proc. Suppl.) **48**, 335 (1996).
- [46] V. Castellani *et al.*, Astron. Astrophys. **271**, 601 (1993); S.A. Bludman *et al.*, Phys. Rev. D **49**, 3622 (1994); V. Berezhinsky, Comm. Nucl. Part. Phys. **21**, 249 (1994); J.N. Bahcall, Phys. Lett. B **338**, 276 (1994).

- [47] S.P. Mikheyev and A.Yu. Smirnov, *Yad. Fiz.* **42**, 1441 (1985) [*Sov. J. Nucl. Phys.* **42**, 913 (1985)]; *Il Nuovo Cimento C* **9**, 17 (1986).
- [48] GALLEX Coll., P. Anselmann *et al.*, *Phys. Lett. B* **285**, 390 (1992); X. Shi, D.N. Schramm and J.N. Bahcall, *Phys. Rev. Lett.* **69**, 717 (1992); P.I. Krastev and S.T. Petcov, *Phys. Lett. B* **299**, 99 (1993); G.L. Fogli and E. Lisi, *Astropart. Phys.* **2**, 91 (1994); N. Hata and P.G. Langacker, *Phys. Rev.* **50**, 632 (1994); G. Fiorentini *et al.*, *ibid.* **49**, 6298 (1994); L.M. Krauss, E. Gates and M. White, *ibid.* **51**, 2631 (1995).
- [49] V. Barger, R.J.N. Phillips, and K. Whisnant, *Phys. Rev. Lett.* **69**, 3135 (1992); P.I. Krastev and S.T. Petcov, *ibid.* **72**, 1960 (1994).
- [50] R.M. Barnett *et al.*, *Phys. Rev. D* **54**, 1 (1996).
- [51] R.G.H. Robertson and D.A. Knapp, *Ann. Rev. Nucl. Part. Sci.* **38**, 185 (1988); N.A. Jelley, *Proc. of the 7th Int. Workshop on Neutrino Telescopes*, Venezia, February 1996, p.131.
- [52] L. Wolfenstein, *Phys. Rev. D* **17**, 2369 (1978); *ibid.* **20**, 2634 (1979).
- [53] E.D. Carlson, *Phys. Rev. D* **34**, 1454 (1986); P.I. Krastev and S.T. Petcov, *Phys. Lett. B* **205**, 84 (1988); G. Auriemma *et al.*, *ibid.* **37**, 665 (1988); E. Akhmedov, P. Lipari and M. Lusignoli, *Phys. Lett. B* **300**, 128 (1993).
- [54] T.K. Kuo and J. Pantaleone, *Rev. Mod. Phys.* **61**, 937 (1989).
- [55] C. Athanassopoulos *et al.*, *Phys. Rev. Lett.* **75**, 2650 (1995); *ibid.* **77**, 3082 (1996).
- [56] C.Y. Cardall and G.M. Fuller, *Phys. Rev. D* **53**, 4421 (1996); O. Yasuda and H. Minakata, preprint TMUP-HEL-9604 (hep-ph/9602386); S.M. Bilenky, C. Giunti and W. Grimus, *Eur. Phys. J. C* **1**, 247 (1998); N. Okada and O. Yasuda, *Int. J. Mod. Phys. A* **12**, 3669 (1997).
- [57] J. Kleinfeller, *Nucl. Phys. B (Proc. Suppl.)* **48**, 207 (1996).
- [58] L. Ludovici and P. Zucchelli, preprint CERN-PPE/96-181; Booster Neutrino Experiment (BooNE), <http://nu1.lampf.lanl.gov/BooNE>.
- [59] F. Boehm, *Nucl. Phys. B (Proc. Suppl.)* **48**, 148 (1996); F. Vannucci, *ibid.* **48**, 154 (1996).
- [60] B. Achkar *et al.*, *Nucl. Phys. B* **434**, 503 (1995).
- [61] G.S. Vidyakin *et al.*, *JETP Lett.* **59**, 390 (1994).
- [62] M. Kobayashi and T. Maskawa, *Prog. Theor. Phys.* **49**, 652 (1973).
- [63] J. Schechter and J.W.F. Valle, *Phys. Rev. D* **21**, 309 (1980); *ibid.* **22**, 2227 (1980).

- [64] S.M. Bilenky, J. Hosek and S.T. Petcov, Phys. Lett. B **94**, 495 (1980).
- [65] I.Yu. Kobzarev *et al.*, Yad. Fiz. **32**, 1590 (1980) [Sov. J. Nucl. Phys. **32**, 823 (1980)].
- [66] M. Doi *et al.*, Phys. Lett. B **102**, 323 (1981).
- [67] P. Langacker *et al.*, Nucl. Phys. B **282**, 589 (1987).
- [68] N. Cabibbo, Phys. Lett. B **72**, 333 (1978).
- [69] F.D. Stacey, *Physics of the Earth*, John Wiley & Sons, Inc., 1977.
- [70] D.L. Anderson, *Theory of the Earth*, Blackwell Scientific Publications, 1989.
- [71] N. Hata and P. Langacker, Phys. Rev. D **56**, 6107 (1997); G.L. Fogli, E. Lisi and D. Montanino, preprint hep-ph/9709473.
- [72] Y. Suzuki (SuperKamiokande), Proc. of the *Fourth International Solar Neutrino Conference*, Heidelberg, Germany, 8–11 April 1997, edited by W. Hampel (Max-Planck-Institut für Kernphysik, 1997), p.163; R. Meijer Drees (SNO), *ibid.*, p.210; F. von Feilitzsch (Borexino), *ibid.*, p.192; E. Bellotti (GNO), *ibid.*, p.173; K. Lande (Homestake Iodine), *ibid.*, p.228; C. Tao (HELLAZ), *ibid.*, p.238; A.V. Kopylov (Lithium), *ibid.*, p.263; Yu.G. Zdesenko (Xenon), *ibid.*, p.283; P. Cennini *et al.* (ICARUS), LNGS-94/99-I, May 1994; T.J. Bowels (GaAs), Proc. of *Neutrino 96*, Helsinki, Finland, 13–19 June 1996, edited by K. Enqvist, K. Huitu and J. Maalampi (World Scientific, Singapore, 1997), p.83.
- [73] A. De Rujula *et al.*, Nucl. Phys. B **168**, 54 (1980); V. Barger and K. Whisnant, Phys. Lett. B **209**, 365 (1988); S.M. Bilenky, M. Fabbrichesi and S.T. Petcov, *ibid.* **276**, 223 (1992).
- [74] S.M. Bilenky *et al.*, Phys. Lett. B **356**, 273 (1995); Phys. Rev. D **54**, 1881 (1996).
- [75] J. Pantaleone, Phys. Rev. D **49**, R2152 (1994).
- [76] J. Pantaleone, private communication and Ref.[75].
- [77] G.L. Fogli and E. Lisi, Phys. Rev. D **52**, 2775 (1995).
- [78] A. Nicolaidis, Phys. Lett. B **200**, 553 (1988).
- [79] F. Dydak *et al.*, Phys. Lett. B **134**, 281 (1984).
- [80] F.D. Murnaghan, *The unitary and rotation groups*, Spartan Books, Washington, D.C. 1962, p.7.

Figure Captions

Figure 1. Density ρ (A) and electron number density (B) in the interior of the Earth as functions of the radial distance r from the center of the Earth. The solid curves represent the data given in Ref.[70]. The electron number density is given by $N_e = N_A(\rho/g)\langle Z/A \rangle$ with $\langle Z/A \rangle = 0.475$ for $r \leq 3480$ Km (core) and $\langle Z/A \rangle = 0.495$ for $r > 3480$ Km (mantle). The dotted curves represent our approximation in terms of five shells with outer radii $r_{i=1,\dots,5} = 1221, 3480, 5701, 5971, 6371$ Km, having constant densities $\rho_{i=1,\dots,5} = 13.0, 11.3, 5.0, 3.9, 3.0$ g/cm³ and electron number density $(N_e)_{i=1,\dots,5} = 6.15, 5.36, 2.47, 1.93, 1.50$ N_A cm⁻³.

Figure 2. Averaged value (2.69b) of the survival probabilities of muon neutrinos (solid curves) and anti-neutrinos (dashed curves) as functions of the distance $L = t$ in a medium with constant electron density $N_e = 3 N_A$ cm⁻³. Two sets of values of the mixing parameters are considered: (A) $|U_{e3}|^2 = |U_{\mu3}|^2 = 1/3$ (which corresponds to maximal mixing of the three neutrinos) and (B) $|U_{e3}|^2 = 0.3, |U_{\mu3}|^2 = 0.5$ (which is close to the best fit of the Kamiokande data; see Eq.(3.6)). The dotted lines represent the averaged survival probabilities in vacuum (2.71), which are equal for neutrinos and anti-neutrinos.

Figure 3. Fig.3A,B: $\langle P_{\nu_\mu \rightarrow \nu_\mu} \rangle$ (solid curves) and $\langle P_{\bar{\nu}_\mu \rightarrow \bar{\nu}_\mu} \rangle$ (dashed curves) for neutrinos propagating in the interior of the Earth as a function of the zenithal angle θ . These figures correspond to the same two sets of values of the mixing parameters as in Fig.2. The dotted lines represent the averaged survival probabilities in vacuum (2.71), which are equal for neutrinos and anti-neutrinos. Fig.3C: slant depth as a function of the zenithal angle θ .

Figure 4. Region in the $B_{e,e}-m_3^2$ plane allowed at 90% CL by the Kamiokande data (the shadowed region). The lightly shadowed region is forbidden by the results of the Bugey [60] and Krasnoyarsk [61] reactor $\bar{\nu}_e$ disappearance experiments, whose exclusion curves are represented by the dashed and dotted lines, respectively. The dash-dotted and dash-dot-dotted curves represent the sensitivity of the CHOOZ [31] and Palo Verde [32] reactor long-baseline experiments.

Figure 5. Region allowed at 90% CL by the Kamiokande data in the $B_{\mu,\mu}-m_3^2$ plane (the shadowed region). The dashed line reproduces the exclusion curve of the CDHS [79] $\bar{\nu}_\mu$ disappearance experiment. The dash-dotted and dash-dot-dotted curves represent the sensitivity of the K2K [33] and MINOS [34] accelerator long-baseline experiments.

Figure 6. Region in the $A_{\mu,e}-m_3^2$ plane allowed at 90% CL by the analysis of the Kamiokande data (the shadowed region). The lightly shadowed region is excluded by the results of the Bugey [60] and Krasnoyarsk [61] reactor neutrino experiments. The long-dashed, dash-dotted and dash-dot-dotted curves represent the sensitivities of the K2K [33], MINOS [34] and ICARUS [35] long-baseline experiments.

Figure 7. Region in the $A_{\mu;\tau}-m_3^2$ plane allowed at 90% CL by the analysis of the Kamiokande data (the shadowed region). The lightly shadowed region is indirectly excluded by the results of the reactor neutrino oscillation experiments, leaving the darkly shadowed allowed region. The dash-dotted and dash-dot-dotted curves represent the sensitivities of the MINOS and ICARUS long-baseline experiments in the $\nu_\mu \rightarrow \nu_\tau$ channel.

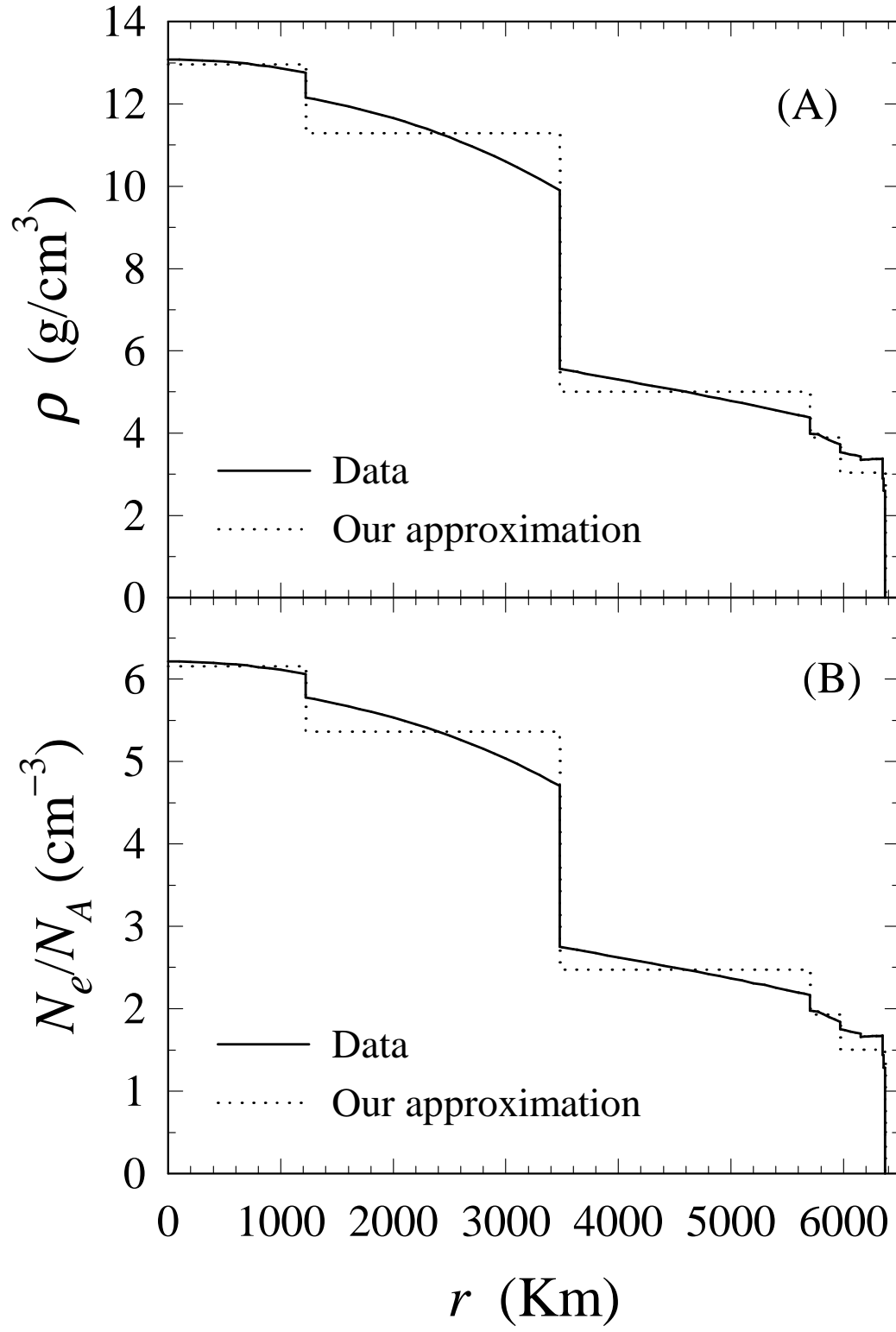


Figure 1

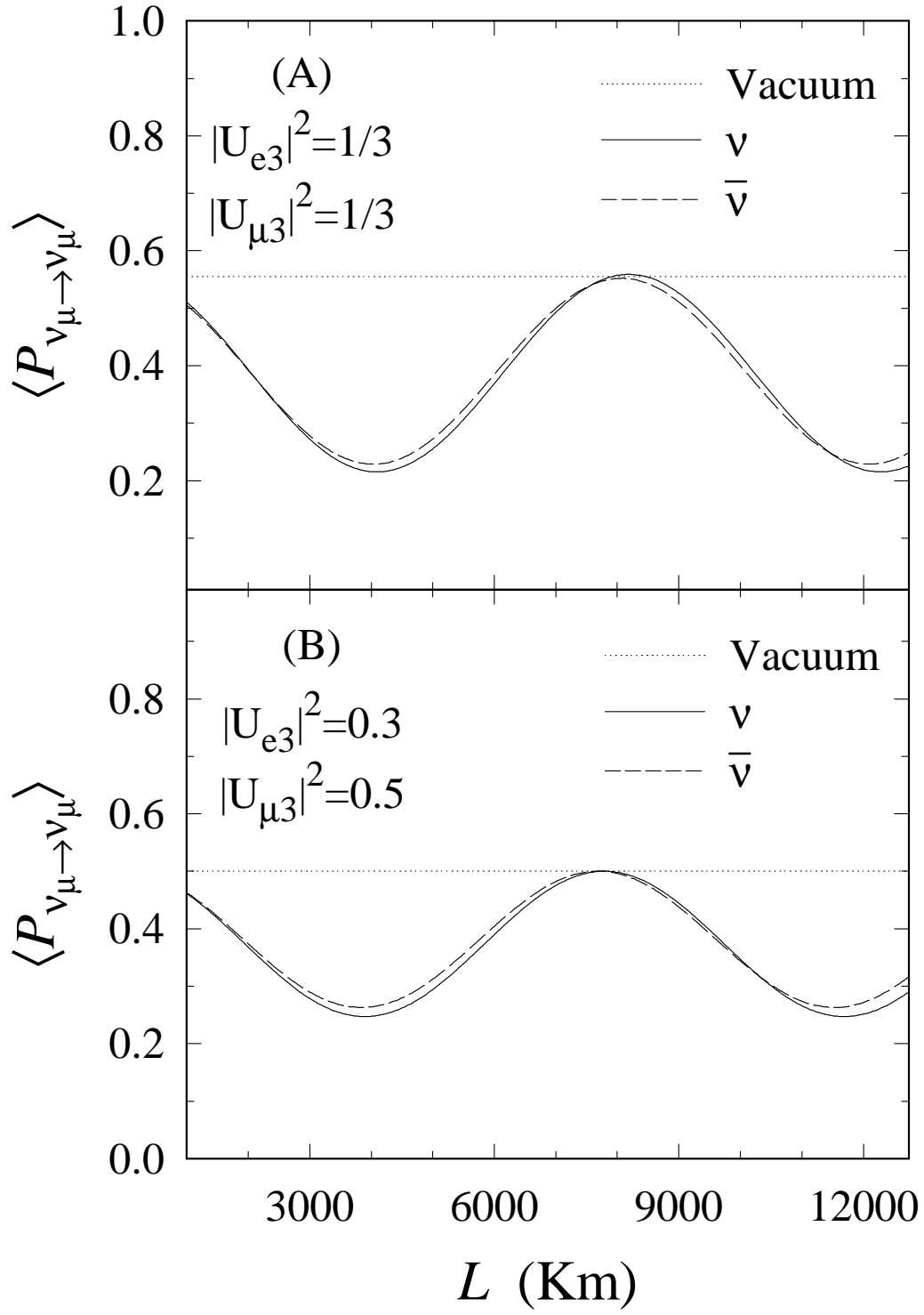


Figure 2

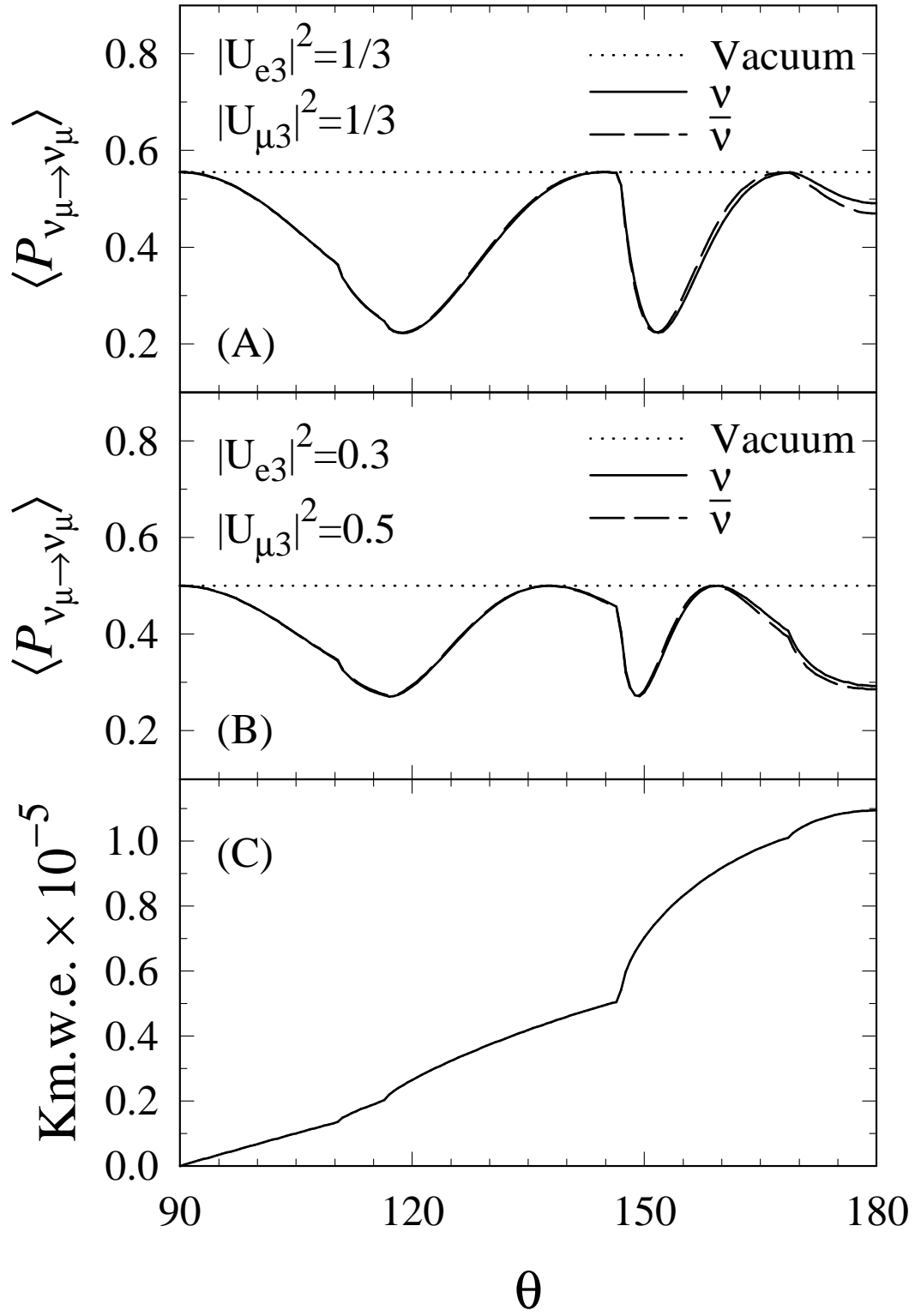


Figure 3

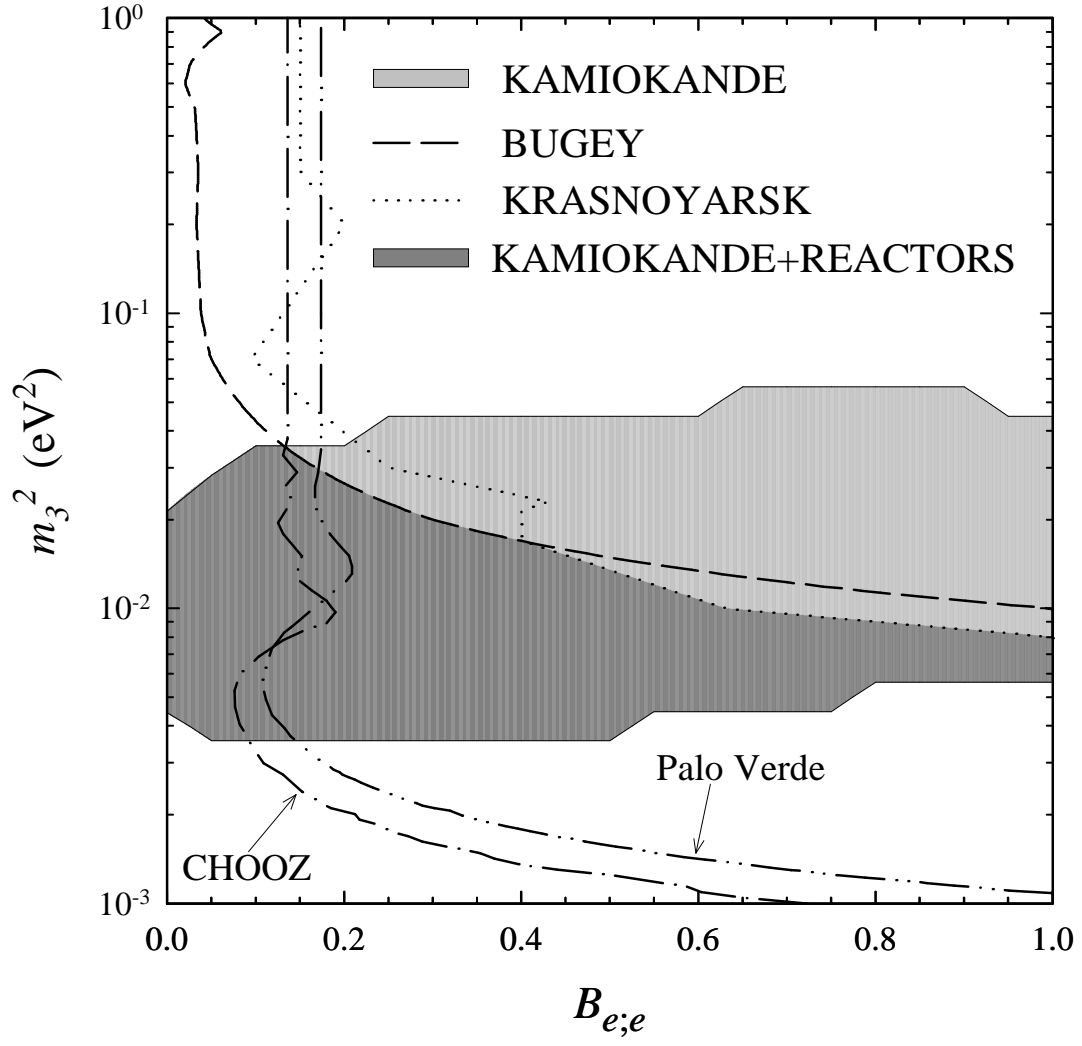


Figure 4

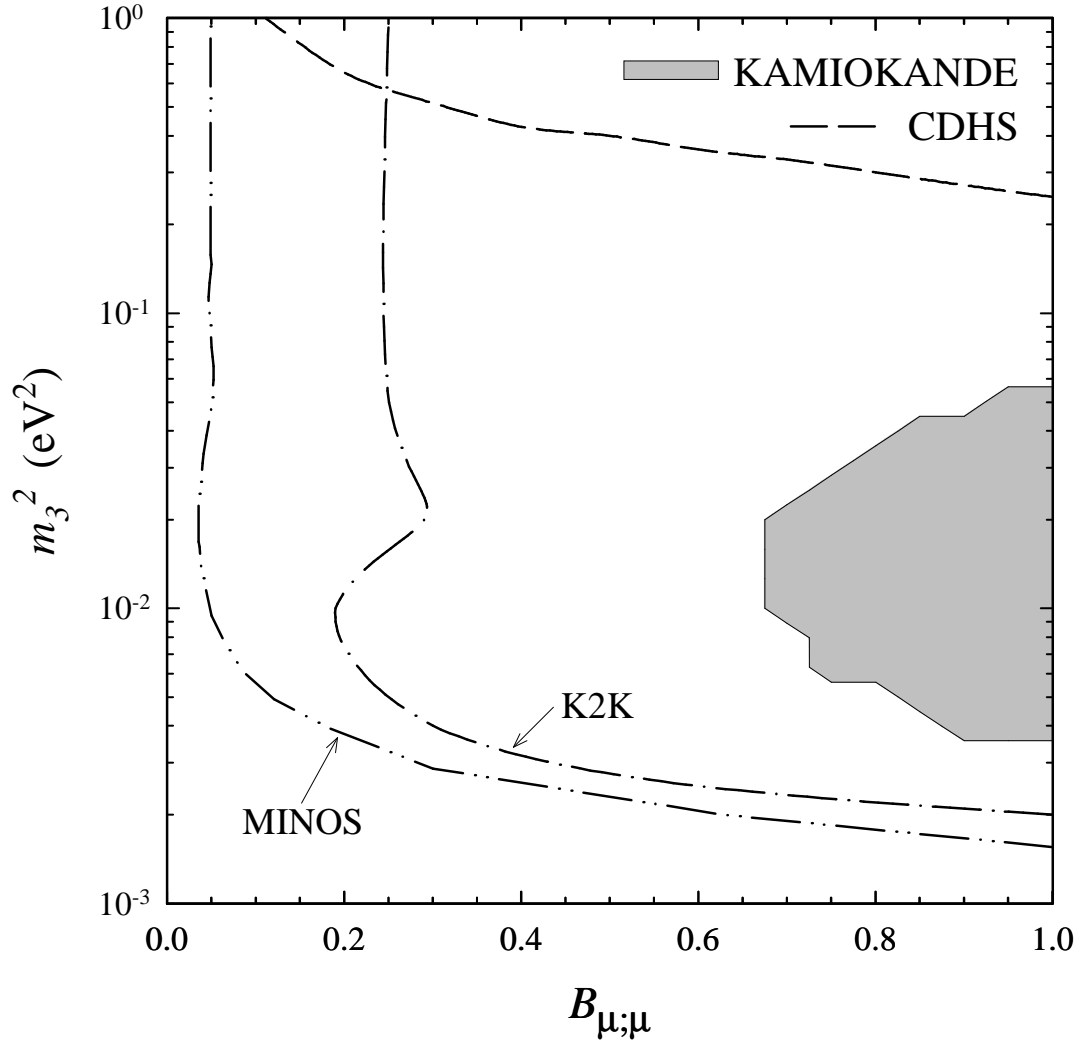


Figure 5

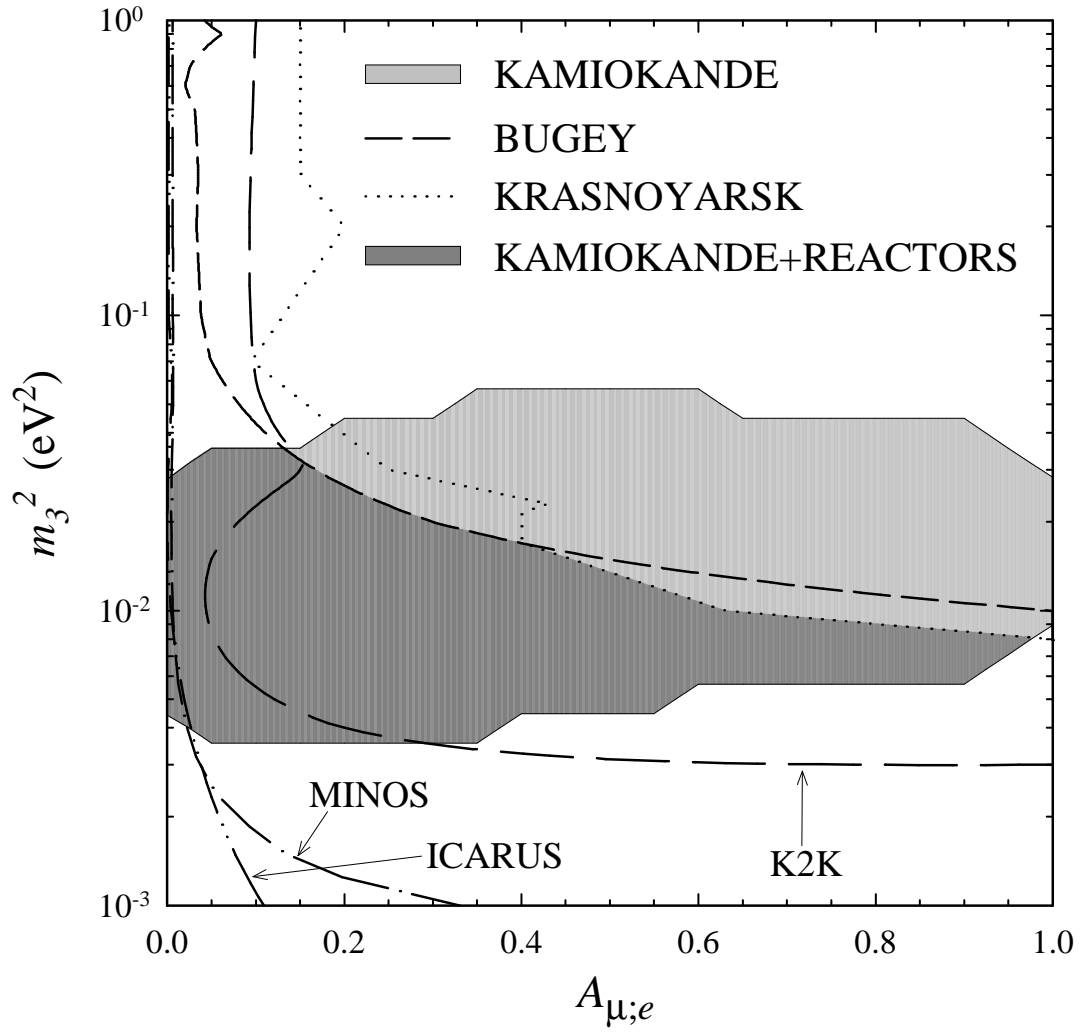


Figure 6

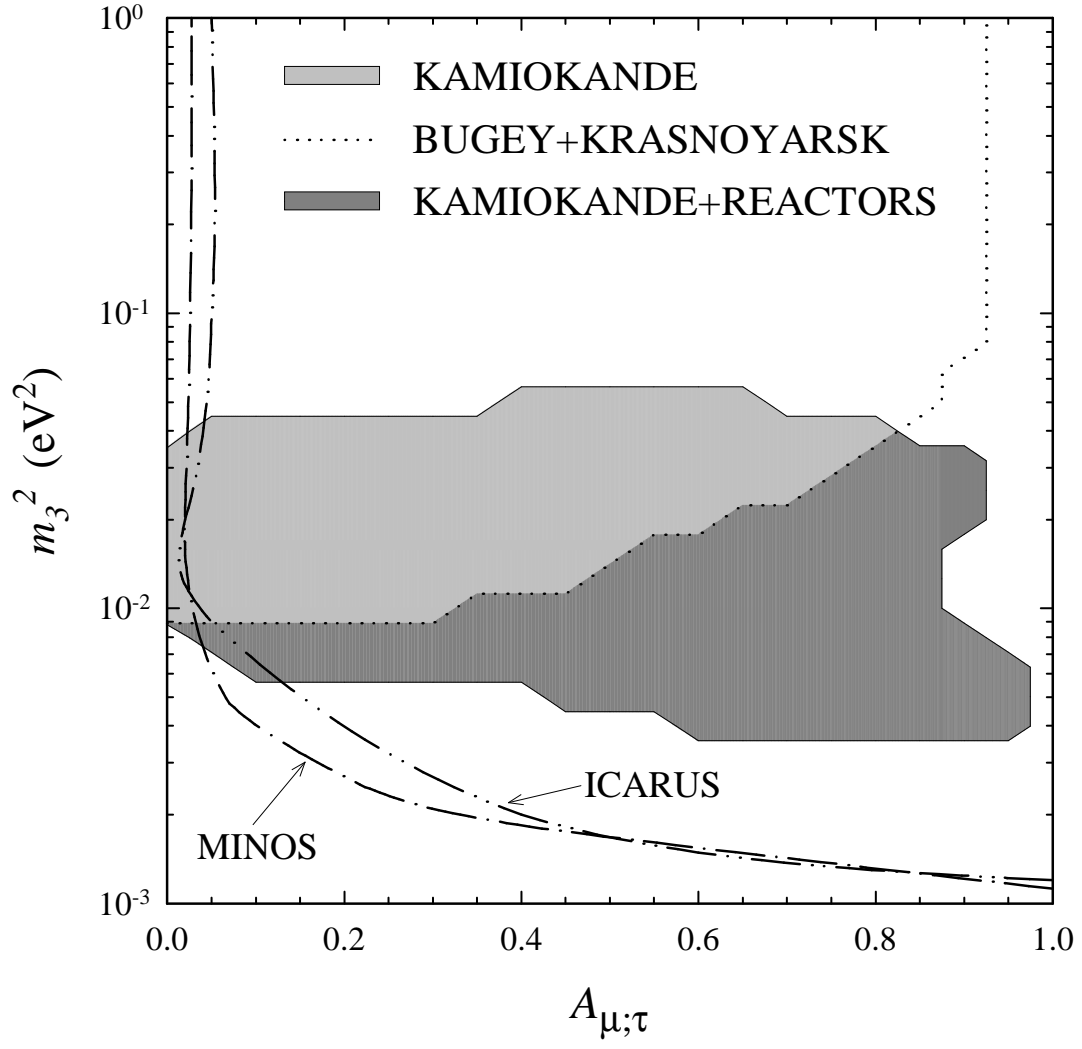


Figure 7